CHAPTER 3. FEEDFORWARD ACTIVE CONTROL OF FLEXURAL VIBRATION IN A PLATE USING PIEZOCERAMIC ACTUATORS AND AN ANGLE STIFFENER

3.1 INTRODUCTION

In this chapter, the active control of flexural vibration in plates using as control sources piezoceramic actuators placed between a stiffener flange and the plate surface is investigated. The plate is rectangular with an angle stiffener mounted across the smaller dimension. The classical equation of motion for the flexural vibration of a plate is used to develop a theoretical model for the plate with primary point sources and an angle stiffener and control actuators (Section 3.2). The effective control signal is a combination of the effects of the point forces at the base of the actuators, and the reaction line force and line moment at the base of the stiffener (Section 3.2.5).

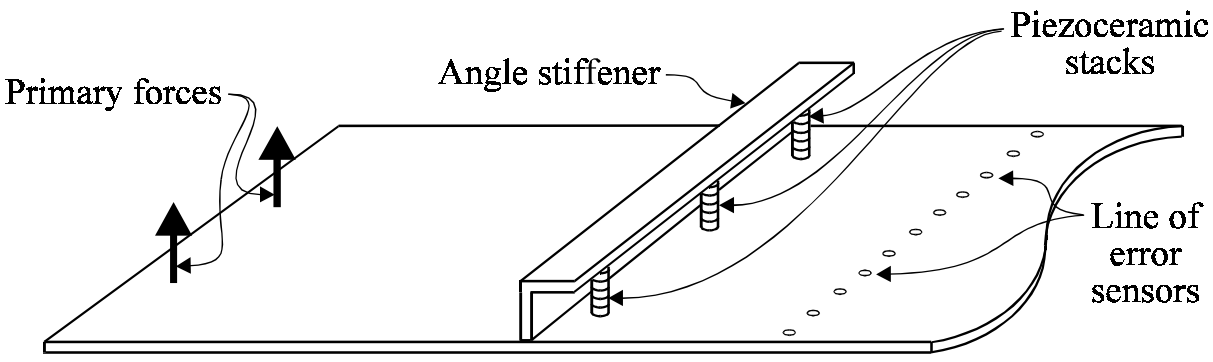

Figure 3.1 Plate showing primary sources, angle stiffener, piezoceramic stack control actuators and error sensors.

The displacement at a point is the sum of the displacements due to each of the primary source and control source forces and moments. Optimal control is achieved by minimising the total mean square displacement at the location of the line of error sensors downstream of the control sources.

The theoretical analysis considers two different sets of plate supports. In both cases, the sides of the plate are modelled as simply supported and the left hand end is modelled as free. In the first case, the right hand end is modelled as infinite and in the second the right hand end is modelled as free. The influence of the control source location, the error sensor location and the excitation frequency on the control source amplitude and achievable attenuation are investigated, and the physical reasons for each observation are explained (Section 3.3). The effect of introducing a second angle stiffener and set of control sources is also examined.

A modal analysis of the plate is performed to show that the stiffener significantly affects the vibration response of the plate. Experimental verification of the theoretical model is performed for the semi-infinite plate with and without active vibration control. The experimental methods are described in Section 3.4. Experimental results are compared with theoretical predictions for the vibration of the plate with and without active vibration control (Section 3.5).

3.2 THEORY

3.2.1 Response of a plate to a harmonic excitation

The response of the plate shown in Figure 3.2 to a simple harmonic excitation $q(x,y)e^{j\omega t}$ is considered. The edges of the plate at $y = 0$ and $y = L_y$ are modelled as simply supported.

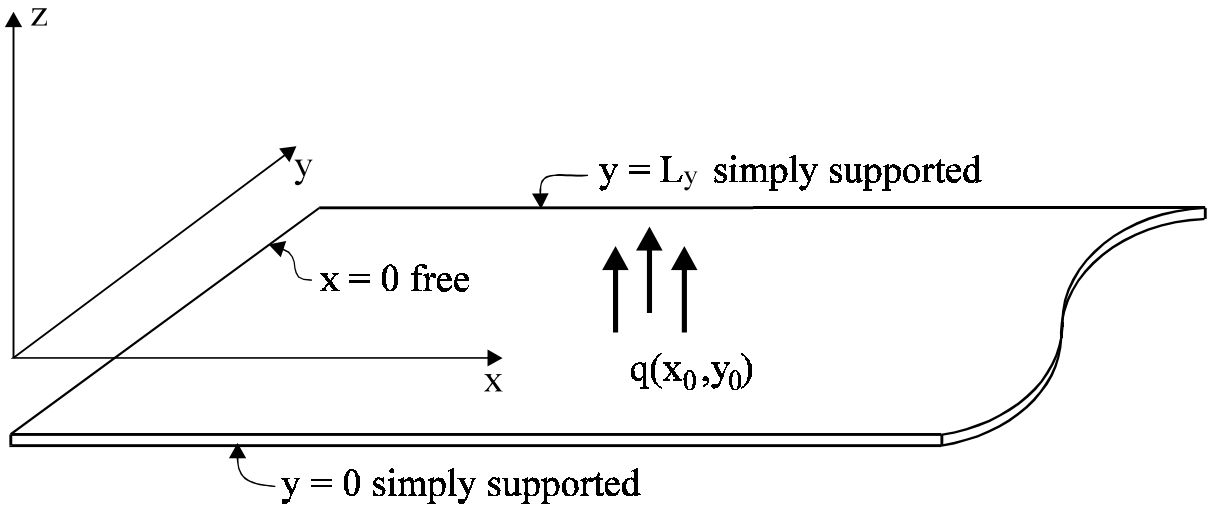

Figure 3.2 Plate with excitation q at location (x_0,y_0).

Following the sign conventions shown in Figure 3.3, the equation of motion for the flexural vibration of the plate shown in Figure 3.2 is (Leissa, 1969)

$$D_h \nabla^4 w(x, y, t) + \rho h \frac{\partial^2 w(x, y, t)}{\partial t^2} = q(x, y)\, e^{j\omega t} \ , \tag{3.1}$$

where $D_h = \frac{Eh^3}{12(1 - \nu^2)}$ is the flexural rigidity, E is Young's modulus of elasticity, h is the plate thickness, ν is Poisson's ratio, ρ is the plate density, t is time, w is displacement, and $\nabla^4 = \nabla^2 \nabla^2$ is the square of the Laplacian operator.

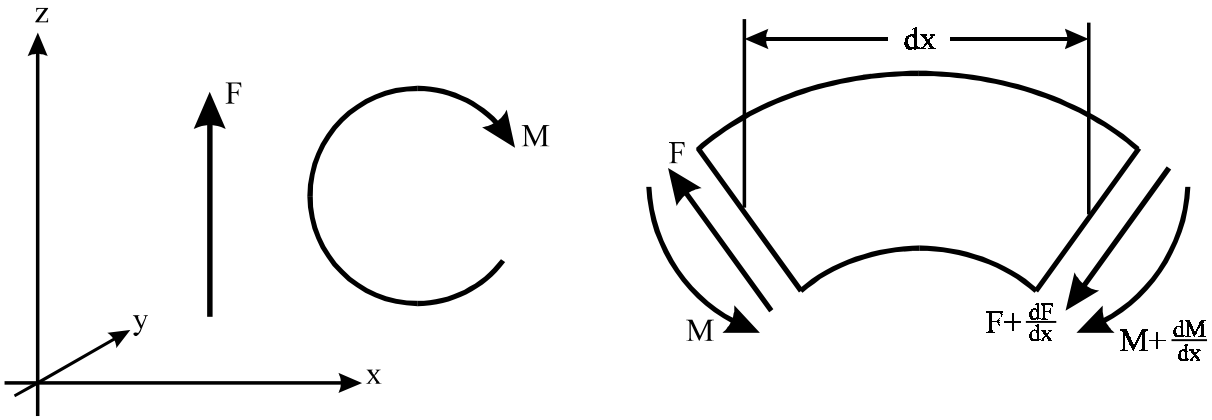

Figure 3.3 Sign conventions for forces and moments. Conventions for moments in the *y*-plane are similar.

As the edges of the plate at $y = 0$ and $y = L_y$ are simply supported, the following harmonic series solution in y can be assumed for the plate vibrational displacement (Pan and Hansen, 1994);

$$w(x, y, t) = \sum_{n=1}^{\infty} w_n(x) \sin\frac{n\pi y}{L_y} e^{j\omega t} , \tag{3.2}$$

where n is a mode number and ω is the angular frequency. Each eigenfunction $w_n(x)$ can be expressed in terms of modal wavenumbers k_{in} as follows:

$$w_n(x) = A_n e^{k_{1n}x} + B_n e^{k_{2n}x} + C_n e^{k_{3n}x} + D_n e^{k_{4n}x} . \tag{3.3}$$

On each side of an applied force or moment at $x = x_0$, the eigenfunction is a different linear combination of the terms $e^{k_{in}x}$ (i = 1,2,3,4). For $x < x_0$,

$$w_{1n}(x) = A_{1n} e^{k_{1n}x} + B_{1n} e^{k_{2n}x} + C_{1n} e^{k_{3n}x} + D_{1n} e^{k_{4n}x} , \tag{3.4}$$

and for $x > x_0$,

$$w_{2n}(x) = A_{2n}e^{k_{1n}x} + B_{2n}e^{k_{2n}x} + C_{2n}e^{k_{3n}x} + D_{2n}e^{k_{4n}x} \ , \tag{3.5}$$

To find the modal wavenumbers k_{in}, the homogeneous form of Equation (3.1) is multiplied by $\sin\frac{n\pi y}{L_y}$ and integrated with respect to y to give

$$\frac{d^4w_n(x)}{dx^4} - 2\left(\frac{n\pi}{L_y}\right)^2\frac{d^2w_n(x)}{dx^2} + \left(\left(\frac{n\pi}{L_y}\right)^4 - \frac{\rho h\omega^2}{D_h}\right)w_n(x) = 0 \ . \tag{3.6}$$

The corresponding characteristic equation is

$$k_n^4 + 2\left(\frac{n\pi}{L_y}\right)^2 k_n^2 + \left(\frac{n\pi}{L_y}\right)^4 - \frac{\rho h\omega^2}{D_h} = 0 \ , \tag{3.7}$$

which has the roots

$$k_{1n,2n} = \pm\left[\left(\frac{n\pi}{L_y}\right)^2 + \left(\frac{\rho h\omega^2}{D_h}\right)^{\frac{1}{2}}\right]^{\frac{1}{2}} \tag{3.8}$$

and

$$k_{3n,4n} = \pm\left[\left(\frac{n\pi}{L_y}\right)^2 - \left(\frac{\rho h\omega^2}{D_h}\right)^{\frac{1}{2}}\right]^{\frac{1}{2}} \ . \tag{3.9}$$

To solve for the eight unknown constants A_{1n}, B_{1n}, C_{1n}, D_{1n}, A_{2n}, B_{2n}, C_{2n} and D_{2n}, eight equations are required, comprising of four boundary condition equations (force and moment

conditions at each end of the plate) and four equilibrium condition equations at the point of application x_0 of the force or moment, for each cross-plate mode n of the plate vibration.

3.2.2 Boundary conditions at the plate ends

For the purposes of this work, two sets of boundary conditions will be examined; those corresponding to a plate with free ends, and to a semi-infinite plate with the end at $x = 0$ modelled as free. Both plates will be modelled with simply supported sides (at $y = 0$ and $y = L_y$).

3.2.2.1 Free end conditions

In terms of displacement, the bending moment boundary condition $M_x(0,y) = 0$ for a free end at $x = 0$ becomes (Pan and Hansen, 1994):

$$\left[k_{1n}^2 - \nu\left(\frac{n\pi}{L_y}\right)^2\right]A_{1n} + \left[k_{2n}^2 - \nu\left(\frac{n\pi}{L_y}\right)^2\right]B_{1n} + \left[k_{3n}^2 - \nu\left(\frac{n\pi}{L_y}\right)^2\right]C_{1n} + \left[k_{4n}^2 - \nu\left(\frac{n\pi}{L_y}\right)^2\right]D_{1n} = 0 \ . \tag{3.10}$$

The corresponding equation for a free end at $x = L_x$ is

$$\left[k_{1n}^2 - \nu\left(\frac{n\pi}{L_y}\right)^2\right]A_{2n}\, e^{k_{1n}L_x} + \left[k_{2n}^2 - \nu\left(\frac{n\pi}{L_y}\right)^2\right]B_{2n}\, e^{k_{2n}L_x} + \left[k_{3n}^2 - \nu\left(\frac{n\pi}{L_y}\right)^2\right]C_{2n}\, e^{k_{3n}L_x} + \left[k_{4n}^2 - \nu\left(\frac{n\pi}{L_y}\right)^2\right]D_{2n} e^{k_{4n}L_x} = 0 \ . \tag{3.11}$$

The free end condition also requires that the net vertical force at the end be zero. This condition yields the following equation in terms of the displacement unknowns for the end $x = 0$,

$$\left[k_{1n}^3 - (2-\nu)\left(\frac{n\pi}{L_y}\right)^2 k_{1n}\right]A_{1n} + \left[k_{2n}^3 - (2-\nu)\left(\frac{n\pi}{L_y}\right)^2 k_{2n}\right]B_{1n} + \left[k_{3n}^3 - (2-\nu)\left(\frac{n\pi}{L_y}\right)^2 k_{3n}\right]C_{1n} + \left[k_{4n}^3 - (2-\nu)\left(\frac{n\pi}{L_y}\right)^2 k_{4n}\right]D_{1n} = 0 \ , \tag{3.12}$$

and for $x = L_x$,

$$\left[k_{1n}^3 - (2-\nu)\left(\frac{n\pi}{L_y}\right)^2 k_{1n}\right]A_{1n}\, e^{k_{1n}L_x} + \left[k_{2n}^3 - (2-\nu)\left(\frac{n\pi}{L_y}\right)^2 k_{2n}\right]B_{1n}\, e^{k_{2n}L_x} + \left[k_{3n}^3 - (2-\nu)\left(\frac{n\pi}{L_y}\right)^2 k_{3n}\right]C_{1n}\, e^{k_{3n}L_x} + \left[k_{4n}^3 - (2-\nu)\left(\frac{n\pi}{L_y}\right)^2 k_{4n}\right]D_{1n}\, e^{k_{4n}L_x} = 0 \ . \tag{3.13}$$

3.2.2.2 Infinite end conditions

An infinite end produces no reflections, so the boundary conditions corresponding to an infinite end at $x = L_x$ are simply

$$A_{2n} = 0 \tag{3.14}$$

and

$$C_{2n} = 0 \ . \tag{3.15}$$

3.2.3 Equilibrium conditions at the point of application ($x = x_0$) of a force or moment

Requiring that the displacement and gradient in each direction be continuous at any point on the plate, the first two equilibrium conditions which must be satisfied at $x = x_0$ are

$$w_{1n} = w_{2n} \tag{3.16}$$

and

$$\frac{\partial w_{1n}}{\partial x} = \frac{\partial w_{2n}}{\partial x} \ . \tag{3.17}$$

The form of the excitation $q(x,y)$ will affect the higher order equilibrium conditions at $x = x_0$. In the following sections the equilibrium conditions corresponding to the plate excited by a point force, a line force parallel to the y-axis, and line moments acting about an axis parallel to the y-axis are discussed. These three types of excitation are induced by an actuator placed between a stiffener flange and the plate.

3.2.3.1 Response of a plate to a point force

The response of the plate to a simple harmonic point force F_0 acting normal to the plate at position (x_0,y_0) is considered. The excitation $q(x,y)$ in Equation (3.1) is replaced by $q(x,y) = F_0\delta(x - x_0)\delta(y - y_0)$, where δ is the Dirac delta function. The second and third order boundary conditions at $x = x_0$ are (Pan and Hansen, 1994):

$$\frac{\partial^2 w_{1n}}{\partial x^2} = \frac{\partial^2 w_{2n}}{\partial x^2} \ , \tag{3.18}$$

and

$$\frac{\partial^3 w_{1n}}{\partial x^3} - \frac{\partial^3 w_{2n}}{\partial x^3} = -\left(\frac{2F_0}{L_y D_h}\right) \sin\frac{n\pi y_0}{L_y} \ . \tag{3.19}$$

3.2.3.2 Response of a plate to a distributed line force parallel to the *y*-axis

Instead of a single point force, the excitation represented by $q(x,y)$ in Equation (3.1) is replaced by an array of N equally spaced point forces distributed along a line parallel to the y-axis between y_1 and y_2. These forces act at locations $(x_0, y_k, k = 1,N)$ and each has a magnitude of F_0/N, so $q(x,y)$ in Equation (3.1) is replaced by $q(x,y) = \left(\frac{F_0}{N}\right) \sum_{k=1}^{N} \delta(x - x_0)\delta(y - y_k)$. The second and third order boundary conditions at $x = x_0$ are

$$\frac{\partial^2 w_{1n}}{\partial x^2} = \frac{\partial^2 w_{2n}}{\partial x^2} \tag{3.20}$$

and

$$\frac{\partial^3 w_{1n}}{\partial x^3} - \frac{\partial^3 w_{2n}}{\partial x^3} = \left(\frac{2F_0}{n\pi(y_2 - y_1)D_h}\right)\left(\cos\frac{n\pi y_2}{L_y} - \cos\frac{n\pi y_1}{L_y}\right) \ . \tag{3.21}$$

3.2.3.3 Response of a plate to a distributed line moment parallel to the *y*-axis

The excitation represented by $q(x,y)$ in Equation (3.1) is replaced by a distributed line moment M_0 per unit length acting along a line parallel to the y-axis between the locations (x_0, y_1) and (x_0,y_2). The excitation term $q(x,y)$ in Equation (3.1) is replaced by $q(x,y) = \frac{\partial M_x}{\partial x} = M_0[\delta'(x - x_0)]\,[h(y - y_1) - h(y - y_2)]$. The second and third order boundary conditions at $x = x_0$ are

$$\frac{\partial^2 w_{1n}}{\partial x^2} - \frac{\partial^2 w_{2n}}{\partial x^2} = \frac{2M_0}{n\pi D_h}\left(\cos\frac{n\pi y_2}{L_y} - \cos\frac{n\pi y_1}{L_y}\right) \tag{3.22}$$

and

$$\frac{\partial^3 w_{1n}}{\partial x^3} = \frac{\partial^3 w_{2n}}{\partial x^3} \ . \tag{3.23}$$

Taking two boundary conditions at each end of the plate from Equations (3.10) - (3.15), the two equilibrium condition Equations (3.16) and (3.17), and two further equilibrium conditions from Equations (3.18) - (3.23), eight equations in the eight unknowns A_{1n}, B_{1n}, C_{1n}, D_{1n}, A_{2n}, B_{2n}, C_{2n} and D_{2n} are obtained. These can be written in the form $\boldsymbol{\alpha X} = \boldsymbol{B}$. The solution vectors $\boldsymbol{X} = [A_{1n}\ B_{1n}\ C_{1n}\ D_{1n}\ A_{2n}\ B_{2n}\ C_{2n}\ D_{2n}]^T = \boldsymbol{\alpha}^{-1}\boldsymbol{B}$ can be used to characterise the response of a plate to simple harmonic excitation by a single point force, a distributed line force along a line parallel to the *y*-axis or a distributed line moment about a line parallel to the *y*-axis.

3.2.4 Modelling the effects of the angle stiffener

The mass and stiffness of the angle stiffener may be significant and are taken into account as follows. Given a plate with an arbitrary excitation q at axial position $x = x_0$ and an angle stiffener extending across the width of the plate at axial position $x = x_1$, as shown in Figure 3.4, three eigenfunction solutions of Equation (3.1) are now required.

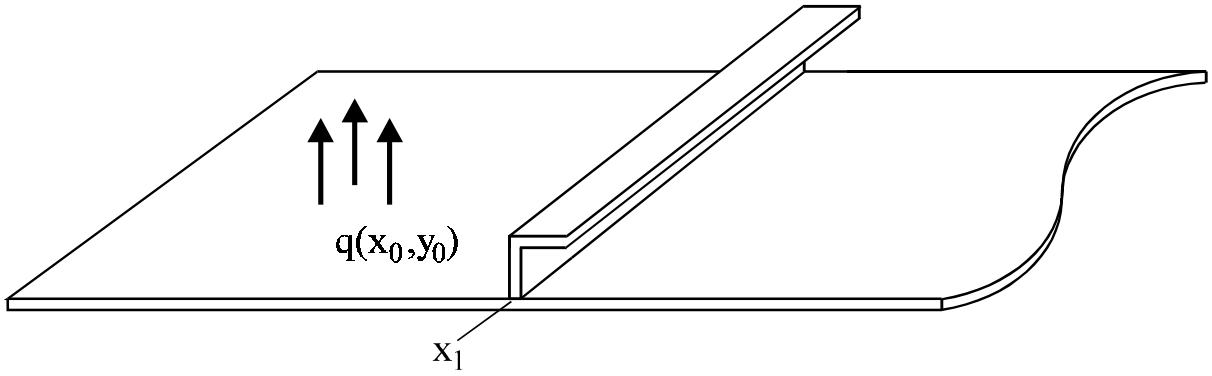

Figure 3.4 Semi-infinite plate with an excitation q and an angle stiffener.

For $x < x_0$,

$$w_{1n}(x) = A_{1n}e^{k_{1n}x} + B_{1n}e^{k_{2n}x} + C_{1n}e^{k_{3n}x} + D_{1n}e^{k_{4n}x} \ , \tag{3.24}$$

for $x_0 < x < x_1$,

$$w_{2n}(x) = A_{2n}e^{k_{1n}x} + B_{2n}e^{k_{2n}x} + C_{2n}e^{k_{3n}x} + D_{2n}e^{k_{4n}x} \ , \tag{3.25}$$

and for $x > x_1$,

$$w_{3n}(x) = A_{3n}e^{k_{1n}x} + B_{3n}e^{k_{2n}x} + C_{3n}e^{k_{3n}x} + D_{3n}e^{k_{4n}x} \ . \tag{3.26}$$

These eigenfunctions allow for reflection at the stiffener location. To solve for $w_{1n}(x)$, $w_{2n}(x)$ and $w_{3n}(x)$, twelve equations in the twelve unknowns $A_{1n}, B_{1n}, C_{1n}, D_{1n}, A_{2n}, B_{2n}, C_{2n}, D_{2n}, A_{3n}$ B_{3n}, C_{3n} and D_{3n} are now required. In addition to the eight equilibrium conditions at $x = x_0$ which depend on the form of the excitation q, and the boundary conditions at each end of the plate, the equilibrium conditions which must be satisfied at the stiffener location $x = x_1$ are

$$w_{2n} = w_{3n} \ , \tag{3.27}$$

$$\frac{\partial w_{2n}}{\partial x} = \frac{\partial w_{3n}}{\partial x} \ , \tag{3.28}$$

$$\frac{\partial^2 w_{2n}}{\partial x^2} = \frac{\partial^2 w_{3n}}{\partial x^2} \ , \tag{3.29}$$

and

$$\frac{\partial^3 w_{2n}}{\partial x^3} - \frac{\partial^3 w_{3n}}{\partial x^3} = \frac{2}{n\pi L_y D_h}\left(K_a w + m_a \frac{\partial^2 w}{\partial t^2} \right)\left(\cos(n\pi) - 1\right) \ , \tag{3.30}$$

where K_a is the stiffness and m_a the mass per unit length of the stiffener. If the angle stiffener is very rigid compared to the plate, Equations (3.27) and (3.30) can be replaced by the two conditions

$$w_2 = 0 \tag{3.31}$$

and

$$w_3 = 0 \ . \tag{3.32}$$

3.2.5 Minimising vibration using piezoceramic actuators and an angle stiffener

For any force or moment excitation, the twelve boundary and equilibrium equations in twelve unknowns can be written in the form $\boldsymbol{\alpha X = B}$, where $\boldsymbol{X} = [A_{1n}, B_{1n}, C_{1n}, D_{1n}, A_{2n}, B_{2n}, C_{2n}, D_{2n}, A_{3n}, B_{3n}, C_{3n}, D_{3n}]^T$ and $\boldsymbol{B}$ is a column vector. When the excitation position is to the left of the stiffener location, i.e. $x_0 < x_1$, $\boldsymbol{B}$ has a non zero excitation term in the seventh row for excitation

by a line moment about a line parallel to the *y*-axis or the eighth row otherwise. For a semi-infinite plate with the end at $x = 0$ free, $\boldsymbol{\alpha}$ is given by Equation (3.33). If the excitation position is to the right of the stiffener location, i.e. $x_0 > x_1$, then a similar analysis is followed, resulting in an excitation vector $\boldsymbol{B}$ with the non zero term in the eleventh row for excitation by a line moment about a line parallel to the *y*-axis or the twelfth row otherwise, and $\boldsymbol{\alpha}$ is given by Equation (3.34). For the plate with both ends modelled as free, the equations corresponding to rows 3 and 4 of the matrix $\boldsymbol{\alpha}$ are replaced by Equations (3.11) and (3.13). For both sets of boundary conditions, the matrix equations $\boldsymbol{\alpha X} = \boldsymbol{B}$ can be solved for $\boldsymbol{X}$ for any type of excitation and the result can be used with Equations (3.2) and (3.24) - (3.26) to calculate the corresponding plate response.

Figure 3.5 shows the semi-infinite plate with primary forces F_{p1} and F_{p2} located at $x = x_p$, $y = y_{p1}$ and $y = y_{p2}$, control actuators at $x = x_c$ and a line of error sensors at $x = x_e$. Figure 3.6 shows the resultant forces and moments applied to the plate by the control actuators. Control forces F_{c1}, F_{c2} and F_{c3} act at (x_{c2}, y_{ci}, $i = 1,3$), with the distributed line force F_c and distributed line moment M_c acting about a line parallel to the *y*-axis at (x_{c1}, $y = 0$ to $y = L_y$).

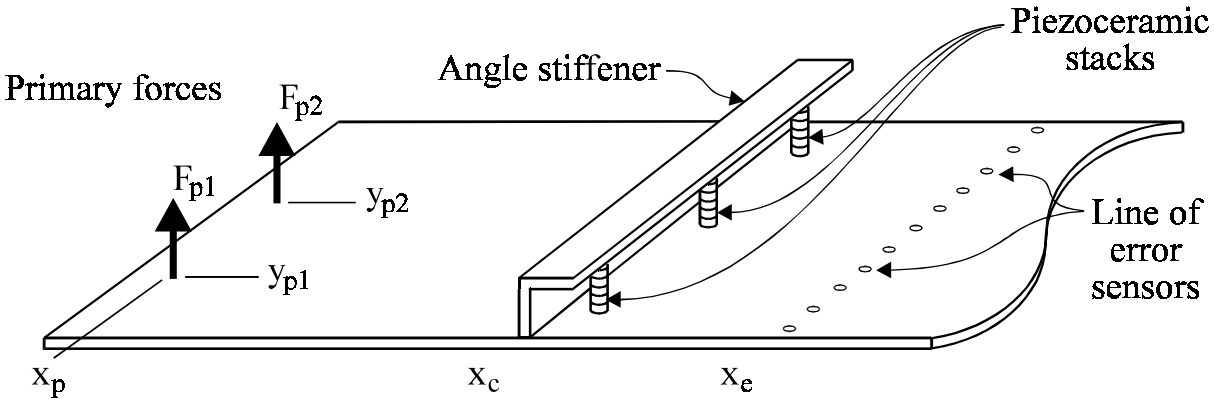

Figure 3.5 Semi-infinite plate showing primary forces, control actuators, angle stiffener and line of error sensors.

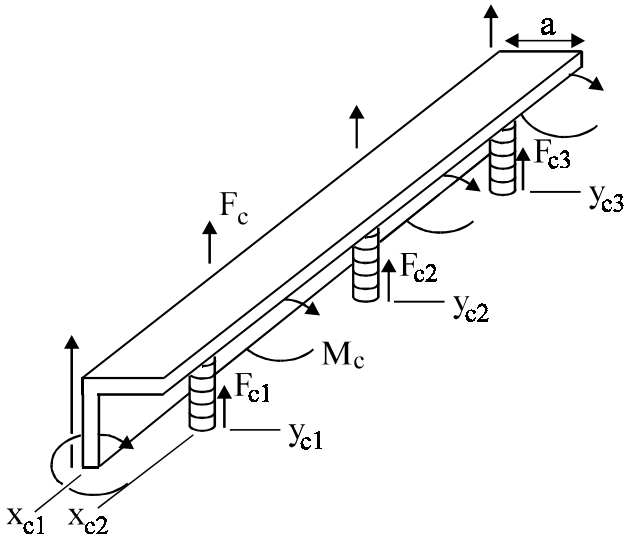

Figure 3.6 Angle stiffener and control actuators showing control forces and moment.

$$\chi = \begin{bmatrix} k_{1n}^2 - \nu\left(\frac{n\pi}{L_y}\right)^2 & k_{2n}^2 - \nu\left(\frac{n\pi}{L_y}\right)^2 & k_{3n}^2 - \nu\left(\frac{n\pi}{L_y}\right)^2 & k_{4n}^2 - \nu\left(\frac{n\pi}{L_y}\right)^2 \\ k_{1n}^3 - (2-\nu)\left(\frac{n\pi}{L_y}\right)^2 k_{1n} & k_{2n}^3 - (2-\nu)\left(\frac{n\pi}{L_y}\right)^2 k_{2n} & k_{3n}^3 - (2-\nu)\left(\frac{n\pi}{L_y}\right)^2 k_{3n} & k_{4n}^3 - (2-\nu)\left(\frac{n\pi}{L_y}\right)^2 k_{4n} \\ 0 & 0 & 0 & 0 \\ 0 & 0 & 0 & 0 \\ e^{k_{1n}x_0} & e^{k_{2n}x_0} & e^{k_{3n}x_0} & e^{k_{4n}x_0} \\ k_{1n}e^{k_{1n}x_0} & k_{2n}e^{k_{2n}x_0} & k_{3n}e^{k_{3n}x_0} & k_{4n}e^{k_{4n}x_0} \\ k_{1n}^2e^{k_{1n}x_0} & k_{2n}^2e^{k_{2n}x_0} & k_{3n}^2e^{k_{3n}x_0} & k_{4n}^2e^{k_{4n}x_0} \\ k_{1n}^3e^{k_{1n}x_0} & k_{2n}^3e^{k_{2n}x_0} & k_{3n}^3e^{k_{3n}x_0} & k_{4n}^3e^{k_{4n}x_0} \\ 0 & 0 & 0 & 0 \\ 0 & 0 & 0 & 0 \\ 0 & 0 & 0 & 0 \\ 0 & 0 & 0 & 0 \end{bmatrix}$$

$$\begin{bmatrix} 0 & 0 & 0 & 0 & 0 & 0 & 0 & 0 \\ 0 & 0 & 0 & 0 & 0 & 0 & 0 & 0 \\ 0 & 0 & 0 & 0 & 1 & 0 & 0 & 0 \\ 0 & 0 & 0 & 0 & 0 & 0 & 1 & 0 \\ -e^{k_{1n}x_0} & -e^{k_{2n}x_0} & -e^{k_{3n}x_0} & -e^{k_{4n}x_0} & 0 & 0 & 0 & 0 \\ -k_{1n}e^{k_{1n}x_0} & -k_{2n}e^{k_{2n}x_0} & -k_{3n}e^{k_{3n}x_0} & -k_{4n}e^{k_{4n}x_0} & 0 & 0 & 0 & 0 \\ -k_{1n}^2e^{k_{1n}x_0} & -k_{2n}^2e^{k_{2n}x_0} & -k_{3n}^2e^{k_{3n}x_0} & -k_{4n}^2e^{k_{4n}x_0} & 0 & 0 & 0 & 0 \\ -k_{1n}^3e^{k_{1n}x_0} & -k_{2n}^3e^{k_{2n}x_0} & -k_{3n}^3e^{k_{3n}x_0} & -k_{4n}^3e^{k_{4n}x_0} & 0 & 0 & 0 & 0 \\ e^{k_{1n}x_1} & e^{k_{2n}x_1} & e^{k_{3n}x_1} & e^{k_{4n}x_1} & 0 & 0 & 0 & 0 \\ 0 & 0 & 0 & 0 & e^{k_{1n}x_1} & e^{k_{2n}x_1} & e^{k_{3n}x_1} & e^{k_{4n}x_1} \\ k_{1n}e^{k_{1n}x_1} & k_{2n}e^{k_{2n}x_1} & k_{3n}e^{k_{3n}x_1} & k_{4n}e^{k_{4n}x_1} & -k_{1n}e^{k_{1n}x_1} & -k_{2n}e^{k_{2n}x_1} & -k_{3n}e^{k_{3n}x_1} & -k_{4n}e^{k_{4n}x_1} \\ k_{1n}^2e^{k_{1n}x_1} & k_{2n}^2e^{k_{2n}x_1} & k_{3n}^2e^{k_{3n}x_1} & k_{4n}^2e^{k_{4n}x_1} & -k_{1n}^2e^{k_{41n}x_1} & -k_{2n}^2e^{k_{2n}x_1} & -k_{3n}^2e^{k_{3n}x_1} & -k_{4n}^2e^{k_{4n}x_1} \end{bmatrix}$$

(3.33)

$$\chi = \begin{bmatrix} k_{1n}^2 - \nu\left(\frac{n\pi}{L_y}\right)^2 & k_{2n}^2 - \nu\left(\frac{n\pi}{L_y}\right)^2 & k_{3n}^2 - \nu\left(\frac{n\pi}{L_y}\right)^2 & k_{4n}^2 - \nu\left(\frac{n\pi}{L_y}\right)^2 \\ k_{1n}^3 - (2-\nu)\left(\frac{n\pi}{L_y}\right)^2 k_{1n} & k_{2n}^3 - (2-\nu)\left(\frac{n\pi}{L_y}\right)^2 k_{2n} & k_{3n}^3 - (2-\nu)\left(\frac{n\pi}{L_y}\right)^2 k_{3n} & k_{4n}^3 - (2-\nu)\left(\frac{n\pi}{L_y}\right)^2 k_{4n} \\ 0 & 0 & 0 & 0 \\ 0 & 0 & 0 & 0 \\ e^{k_{1n}x_1} & e^{k_{2n}x_1} & e^{k_{3n}x_1} & e^{k_{4n}x_1} \\ 0 & 0 & 0 & 0 \\ k_{1n}e^{k_{1n}x_1} & k_{2n}e^{k_{2n}x_1} & k_{3n}e^{k_{3n}x_1} & k_{4n}e^{k_{4n}x_1} \\ k_{1n}^2 e^{k_{1n}x_1} & k_{2n}^2 e^{k_{2n}x_1} & k_{3n}^2 e^{k_{3n}x_1} & k_{4n}^2 e^{k_{4n}x_1} \\ 0 & 0 & 0 & 0 \\ 0 & 0 & 0 & 0 \\ 0 & 0 & 0 & 0 \\ 0 & 0 & 0 & 0 \end{bmatrix}$$

$$\begin{bmatrix} 0 & 0 & 0 & 0 & 0 & 0 & 0 & 0 \\ 0 & 0 & 0 & 0 & 0 & 0 & 0 & 0 \\ 0 & 0 & 0 & 0 & 1 & 0 & 0 & 0 \\ 0 & 0 & 0 & 0 & 0 & 0 & 1 & 0 \\ 0 & 0 & 0 & 0 & 0 & 0 & 0 & 0 \\ e^{k_{1n}x_1} & e^{k_{2n}x_1} & e^{k_{3n}x_1} & e^{k_{4n}x_1} & 0 & 0 & 0 & 0 \\ -k_{1n}e^{k_{1n}x_1} & -k_{2n}e^{k_{2n}x_1} & -k_{3n}e^{k_{3n}x_1} & -k_{4n}e^{k_{4n}x_1} & 0 & 0 & 0 & 0 \\ -k_{1n}^2 e^{k_{1n}x_1} & -k_{2n}^2 e^{k_{2n}x_1} & -k_{3n}^2 e^{k_{3n}x_1} & -k_{4n}^2 e^{k_{4n}x_1} & 0 & 0 & 0 & 0 \\ e^{k_{1n}x_0} & e^{k_{2n}x_0} & e^{k_{3n}x_0} & e^{k_{4n}x_0} & -e^{k_{1n}x_0} & -e^{k_{2n}x_0} & -e^{k_{3n}x_0} & -e^{k_{4n}x_0} \\ k_{1n}e^{k_{1n}x_0} & k_{2n}e^{k_{2n}x_0} & k_{3n}e^{k_{3n}x_0} & k_{4n}e^{k_{4n}x_0} & -k_{1n}e^{k_{1n}x_0} & -k_{2n}e^{k_{2n}x_0} & -k_{3n}e^{k_{3n}x_0} & -k_{4n}e^{k_{4n}x_0} \\ k_{1n}^2 e^{k_{1n}x_0} & k_{2n}^2 e^{k_{2n}x_0} & k_{3n}^2 e^{k_{3n}x_0} & k_{4n}^2 e^{k_{4n}x_0} & -k_{1n}^2 e^{k_{1n}x_0} & -k_{2n}^2 e^{k_{2n}x_0} & -k_{3n}^2 e^{k_{3n}x_0} & -k_{4n}^2 e^{k_{4n}x_0} \\ k_{1n}^3 e^{k_{1n}x_0} & k_{2n}^3 e^{k_{2n}x_0} & k_{3n}^3 e^{k_{3n}x_0} & k_{4n}^3 e^{k_{4n}x_0} & -k_{1n}^3 e^{k_{1n}x_0} & -k_{2n}^3 e^{k_{2n}x_0} & -k_{3n}^3 e^{k_{3n}x_0} & -k_{4n}^3 e^{k_{4n}x_0} \end{bmatrix}$$

(3.34)

The plate response amplitude at any location (x,y) to a particular excitation located at x_0, with an angle stiffener across the width of the plate at location x_1 is

$$w(x,y) = \sum_{n=1}^{\infty} [\boldsymbol{X}^T \boldsymbol{E}(x)] \sin\frac{n\pi y}{L_y} , \tag{3.35}$$

where, for $x < x_0$ and $x < x_1$,

$$\boldsymbol{E}(x) = \left[e^{k_{1n}x} \;\; e^{k_{2n}x} \;\; e^{k_{3n}x} \;\; e^{k_{4n}x} \;\; 0 \;\; 0 \;\; 0 \;\; 0 \;\; 0 \;\; 0 \;\; 0 \;\; 0\right]^T , \tag{3.36}$$

for $x_0 < x < x_1$ or $x_1 < x < x_0$,

$$\boldsymbol{E}(x) = \left[0 \;\; 0 \;\; 0 \;\; 0 \;\; e^{k_{1n}x} \;\; e^{k_{2n}x} \;\; e^{k_{3n}x} \;\; e^{k_{4n}x} \;\; 0 \;\; 0 \;\; 0 \;\; 0\right]^T , \tag{3.37}$$

and for $x > x_0$ and $x > x_1$,

$$\boldsymbol{E}(x) = \left[0 \;\; 0 \;\; 0 \;\; 0 \;\; 0 \;\; 0 \;\; 0 \;\; 0 \;\; e^{k_{1n}x} \;\; e^{k_{2n}x} \;\; e^{k_{3n}x} \;\; e^{k_{4n}x}\right]^T . \tag{3.38}$$

By summation of the displacement equations calculated for each force and moment, the total plate displacement resulting from the primary and control excitations is

$$\begin{aligned} w &= \sum_{i=1}^{2} \left(w_{F_{pi}}\right) + \sum_{i=1}^{3} \left(w_{F_{ci}}\right) + w_{F_c} + w_{M_c} \\ &\sum_{n=1}^{\infty} \left(\sum_{i=1}^{2} \left[\boldsymbol{X}_{\boldsymbol{F_{pi}}}^{\boldsymbol{T}} \boldsymbol{E}(x)\right] + \sum_{i=1}^{3} \left[\boldsymbol{X}_{\boldsymbol{F_{ci}}}^{\boldsymbol{T}} \boldsymbol{E}(x)\right] + \boldsymbol{X}_{\boldsymbol{F_c}}^{\boldsymbol{T}} \boldsymbol{E}(x) + \boldsymbol{X}_{\boldsymbol{M_c}}^{\boldsymbol{T}} \boldsymbol{E}(x) \right) \sin \end{aligned} \tag{3.39}$$

where the subscripts F_{pi}, F_{ci}, F_c and M_c on w and $\boldsymbol{X}$ refer to the corresponding excitation force or moment.

As the excitation vector $\boldsymbol{B}$ has a non-zero element in one row only, the solution vector $\boldsymbol{X}$ can be written in terms of a single column of the inverse matrix $\boldsymbol{\alpha}^{-1}$:

$$\boldsymbol{X} = (\boldsymbol{\alpha}^{-1})_{k,8} B_8 \ , \quad (\boldsymbol{\alpha}^{-1})_{k,11} B_{11} \quad or \quad (\boldsymbol{\alpha}^{-1})_{k,12} B_{12} \ , \ k = 1,12 \ , \tag{3.40}$$

where $(\boldsymbol{\alpha}^{-1})_{k,i}$ is the k^{th} element in the i^{th} column of the inverse of $\boldsymbol{\alpha}$ and B_i is the i^{th} element (the non-zero element) of $\boldsymbol{B}$. The value taken by i depends on the form and location of the excitation, as discussed previously.

3.2.5.1 Control sources driven by the same signal

If the three control actuators are driven by the same signal, then the actuator forces are $F_{c1} = F_{c2} = F_{c3} = -F_s$, say. Also, if the angle stiffener is rigid compared to the plate, the line force $F_c = 3F_s$ and the line moment $M_c = -3aF_s$, where a is the width of the stiffener flange. If the two primary shakers are driven by the same signal, then the primary forces are $F_{p1} = F_{p2} = F_p$. Defining

$$\boldsymbol{F_{Pi}} = \frac{-2}{L_y D_h} \left\langle \boldsymbol{\alpha}^{-1}_{\boldsymbol{F_{pi}}} \right\rangle^T_{k,8} \qquad (i = 1,2) \ , \tag{3.41}$$

$$\boldsymbol{F_{Ci}} = \frac{-2}{L_y D_h} \left\langle \boldsymbol{\alpha}^{-1}_{\boldsymbol{F_{ci}}} \right\rangle^T_{k,12} \qquad (i = 1,3) \ , \tag{3.42}$$

$$\boldsymbol{F_C} = \frac{-2}{\pi L_y D_h} \left\langle \boldsymbol{\alpha}^{-1}_{\boldsymbol{F_c}} \right\rangle^T_{k,12} \ , \tag{3.43}$$

and

$$\boldsymbol{M_C} = \frac{2}{\pi D_h}\left(\boldsymbol{\alpha}_{\boldsymbol{M_c}}^{-1}\right)_{k,11}^{T} , \tag{3.44}$$

and substituting Equations (3.41)-(3.44) into Equation (3.39) and rearranging gives

$$w(x,y) = \sum_{n=1}^{\infty} \left\{ \left[\sum_{i=1}^{2} -\boldsymbol{F_{Pi}} \sin\frac{n\pi y_{pi}}{L_y} \right] F_p + \left[\left(\sum_{i=1}^{3} -\boldsymbol{F_{Ci}} \sin\frac{n\pi y_{ci}}{L_y} \right) + \left(\frac{3\boldsymbol{F_C} - 3x_a \boldsymbol{M_C}}{n} \right) (1 - \cos n\pi) \right] F_s \right\} \boldsymbol{E}(x) \sin\frac{n\pi y}{L_y} , \tag{3.45}$$

or

$$w(x,y) = w_p(x,y)\, F_p + w_s(x,y)\, F_s , \tag{3.46}$$

where

$$w_p(x,y) = \sum_{n=1}^{\infty} \left[\sum_{i=1}^{2} -F_{Pi} \sin\frac{n\pi y_{pi}}{L_y} \right] \boldsymbol{E}(x) \sin\frac{n\pi y}{L_y} \tag{3.47}$$

and

$$w_s(x,y) = \sum_{n=1}^{\infty} \left[\left(\sum_{i=1}^{3} -\boldsymbol{F_{ci}} \sin\frac{n\pi y_{ci}}{L_y} \right) + \left(\frac{3\boldsymbol{G_C} - 3x_a \boldsymbol{M_C}}{n} \right) (1 - \cos n\pi) \right] \boldsymbol{E}(x) \sin\frac{n\pi y}{L_y} . \tag{3.48}$$

The radial acceleration at the line $x = x_e$ is to be minimised. The mean square of the

displacement defined in Equation (3.46) is integrated over the width of the plate:

$$\int_0^{L_y} |w(x_e,y)|^2 dy = \int_0^{L_y} |F_p w_p(x_e,y) + F_s w_s(x_e,y)|^2 dy \ . \tag{3.49}$$

Noting that $|z|^2 = z\bar{z}$ (where $\bar{z}$ is the complex conjugate of z), and writing $F_s = F_{sr} + F_{sj}j$,

$$\begin{aligned}\int_0^{L_y} |w(x_e,y)|^2 dy = \int_0^{L_y} \Big(&|F_p|^2 |w_p|^2 + F_p w_p \overline{w_s}(F_{sr} - F_{sj}j) + \\ &\overline{F_p w_p} w_s (F_{sr} + F_{sj}j) + (F_{sr}^2 + F_{sj}^2)|w_s|^2 \Big) dy \ .\end{aligned} \tag{3.50}$$

The partial derivatives of Equation (3.50) with respect to the real and imaginary components of the control force are taken and set equal to zero to find

$$\frac{\partial(\ \ )}{\partial F_{sr}} = \int_0^{L_y} \Big(F_p w_p \overline{w_s} + \overline{F_p w_p} w_s + 2F_{sr}|w_s|^2 \Big) dy = 0 \tag{3.51}$$

and

$$j\frac{\partial(\ \ )}{\partial F_{sj}} = \int_0^{L_y} \Big(F_p w_p \overline{w_s} - \overline{F_p w_p} w_s + 2jF_{sj}|w_s|^2 \Big) dy = 0 \ . \tag{3.52}$$

Adding Equations (3.51) and (3.52) gives

$$\int_0^{L_y} \Big(F_p w_p \overline{w_s} + F_s |w_s|^2 \Big) dy = 0 \ . \tag{3.53}$$

The optimal control force F_s required to minimise normal acceleration at the ring of error sensors

can thus be calculated by

$$F_s = -F_p \frac{\int_0^{L_y} w_p(x_e,\theta)\,\overline{w_s(x_e,\theta)}\,dy}{\int_0^{L_y} |w_s(x_e,\theta)|^2 dy} \,. \tag{3.54}$$

3.2.5.2 Control sources driven independently

If the three control actuators are driven independently, then a similar analysis is followed; however, three equations instead of one result from integrating the mean square of the displacement defined in Equation (3.46) and setting the partial derivatives of the integration with respect to the real and imaginary components of each control force equal to zero. The optimal control forces F_{s1}, F_{s2} and F_{s3} required to minimise acceleration at the line of error sensors can be calculated by

$$\begin{bmatrix} F_{s1} \\ F_{s2} \\ F_{s3} \end{bmatrix} = -F_p \begin{bmatrix} \int_0^{L_y} w_1\overline{w_1}dy & \int_0^{L_y} w_2\overline{w_1}dy & \int_0^{L_y} w_3\overline{w_1}dy \\ \int_0^{L_y} w_1\overline{w_2}dy & \int_0^{L_y} w_2\overline{w_2}dy & \int_0^{L_y} w_3\overline{w_2}dy \\ \int_0^{L_y} w_1\overline{w_3}dy & \int_0^{L_y} w_2\overline{w_3}dy & \int_0^{L_y} w_3\overline{w_3}dy \end{bmatrix}^{-1} \begin{bmatrix} \int_0^{L_y} w_p\overline{w_1}dy \\ \int_0^{L_y} w_p\overline{w_2}dy \\ \int_0^{L_y} w_p\overline{w_3}dy \end{bmatrix} . \tag{3.55}$$

3.2.5.3 Two angle stiffeners and two sets of control sources

If a second set of three control sources and an additional angle stiffener are introduced at some location $x_c^{/}$ downstream from the first, and a prime used to denote values associated with the second set of control sources, the optimal control forces $F_{s1}^{/}$, $F_{s2}^{/}$ and $F_{s3}^{/}$ required to minimise acceleration at the line of error sensors can be calculated by

$$\begin{bmatrix} F_{s1}^{/} \\ F_{s2}^{/} \\ F_{s3}^{/} \end{bmatrix} = \begin{bmatrix} \int_0^{L_y} w_1^{/}\overline{w_1^{/}}dy & \int_0^{L_y} w_2^{/}\overline{w_1^{/}}dy & \int_0^{L_y} w_3^{/}\overline{w_1^{/}}dy \\ \int_0^{L_y} w_1^{/}\overline{w_2^{/}}dy & \int_0^{L_y} w_2^{/}\overline{w_2^{/}}dy & \int_0^{L_y} w_3^{/}\overline{w_2^{/}}dy \\ \int_0^{L_y} w_1^{/}\overline{w_3^{/}}dy & \int_0^{L_y} w_2^{/}\overline{w_3^{/}}dy & \int_0^{L_y} w_3^{/}\overline{w_3^{/}}dy \end{bmatrix}^{-1} \begin{bmatrix} \int_0^{L_y} \left(F_p w_p + F_{s1} w_1 + F_{s2} w_2 + F_{s3} w_3\right)\overline{w_1^{/}}dy \\ \int_0^{L_y} \left(F_p w_p + F_{s1} w_1 + F_{s2} w_2 + F_{s3} w_3\right)\overline{w_2^{/}}dy \\ \int_0^{L_y} \left(F_p w_p + F_{s1} w_1 + F_{s2} w_2 + F_{s3} w_3\right)\overline{w_3^{/}}dy \end{bmatrix}. \tag{3.56}$$

3.2.5.4 Discrete error sensors

If the sum of the squares of the vibration amplitude measured at Q discrete points (x_e, y_{qe}), $q = 1, Q$ is used as the error signal instead of the integral over the plate width at location x_e, Equation (3.55) becomes

$$\begin{bmatrix} F_{s1} \\ F_{s2} \\ F_{s3} \end{bmatrix} = -F_p \begin{bmatrix} \sum_{q=1}^{Q} w_1\overline{w_1} & \sum_{q=1}^{Q} w_2\overline{w_1} & \sum_{q=1}^{Q} w_3\overline{w_1} \\ \sum_{q=1}^{Q} w_1\overline{w_2} & \sum_{q=1}^{Q} w_2\overline{w_2} & \sum_{q=1}^{Q} w_3\overline{w_2} \\ \sum_{q=1}^{Q} w_1\overline{w_3} & \sum_{q=1}^{Q} w_2\overline{w_3} & \sum_{q=1}^{Q} w_3\overline{w_3} \end{bmatrix}^{-1} \begin{bmatrix} \sum_{q=1}^{Q} w_p\overline{w_1} \\ \sum_{q=1}^{Q} w_p\overline{w_2} \\ \sum_{q=1}^{Q} w_p\overline{w_3} \end{bmatrix}, \tag{3.57}$$

where

$$w_i = w_i(x_e, y_{qe}) \ . \tag{3.58}$$

3.3 NUMERICAL RESULTS

The theoretical model developed in the previous section was programmed in Fortran. The program consisted of about 1800 lines and, for a typical set of results, took two or three hours C.P.U. time to run on a SPARC-20 computer.

The discussion that follows examines the effect of varying forcing frequency, control source location and error sensor location on the active control of vibration in plates with two sets of boundary conditions. In both models the sides of the plate at $y = 0$ and $y = L_y$ are modelled as pinned and the end at $x = 0$ is modelled as free. In one model, the end at $x = L_x$ is also modelled as free and in the second model the plate is modelled as semi-infinite in the x-direction. The plate parameters (including location of the control source, primary source and error sensor) are listed in Table 3.1. These values are adhered to unless otherwise stated. The stiffener was assumed to be very stiff in comparison to the plate.

Control forces are expressed as a multiple of the primary force, and the acceleration amplitude dB scale reference level is the far field uncontrolled infinite plate acceleration produced by the primary sources only. In all cases, the control forces are assumed to be optimally adjusted to minimise the acceleration at the line of error sensors. The flexural wavelength of vibration in a plate is given by

$$\lambda_b = \frac{1}{f}\left(\frac{E_y h^2 \omega^2}{12\rho(1 - \nu^2)} \right)^{\frac{1}{4}} . \tag{3.59}$$

Table 3.1

Plate Parameters for Numerical and Experimental Results

Parameter	Value
Plate length L_x	2.0 m
Plate width L_y	0.50 m
Plate thickness h	0.003 m
Young's modulus E	210 GPa
Primary source location x_p	0.025 m
Primary source locations y_{p1}, y_{p2}	0.17m, 0.33m
Control source location x_1	0.5 m (=1.39λ_b)*
Control source locations y_{c1}, y_{c2}, y_{c3}	0.08m, 0.25m, 0.42m
Stiffener flange length a	0.05 m
Error sensor location x_e	1.0 m (= 2.79λ_b)*
Excitation frequency f	230 Hz
Wavelength λ_b	0.359 m*

* - Applies only when f = 230 Hz.

3.3.1 Acceleration distributions for controlled and uncontrolled cases

Figures 3.7 and 3.8 show the uncontrolled acceleration amplitude distribution in dB for the semi-infinite and finite plates. The shape of the curve downstream of the angle stiffener location (x_{c1} = 0.5m) represents a travelling wave field with an additional decaying evanescent field close to the source. Waves reflected from the stiffener and the plate ends cause standing wave fields to exist, both upstream and downstream of the angle stiffener for the finite plate and upstream of the stiffner for the semi-infinte plate.

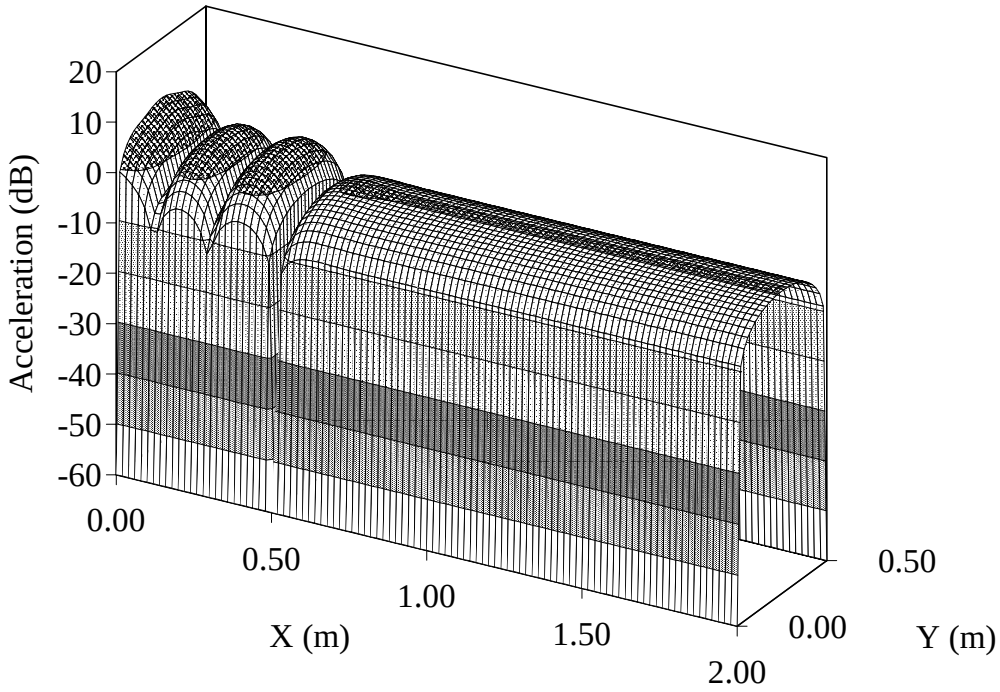

Figure 3.7 Uncontrolled semi-infinite plate acceleration distribution. The edges $y = 0$ and $y = 0.5$ are simply supported and the end at $x = 0$ is free.

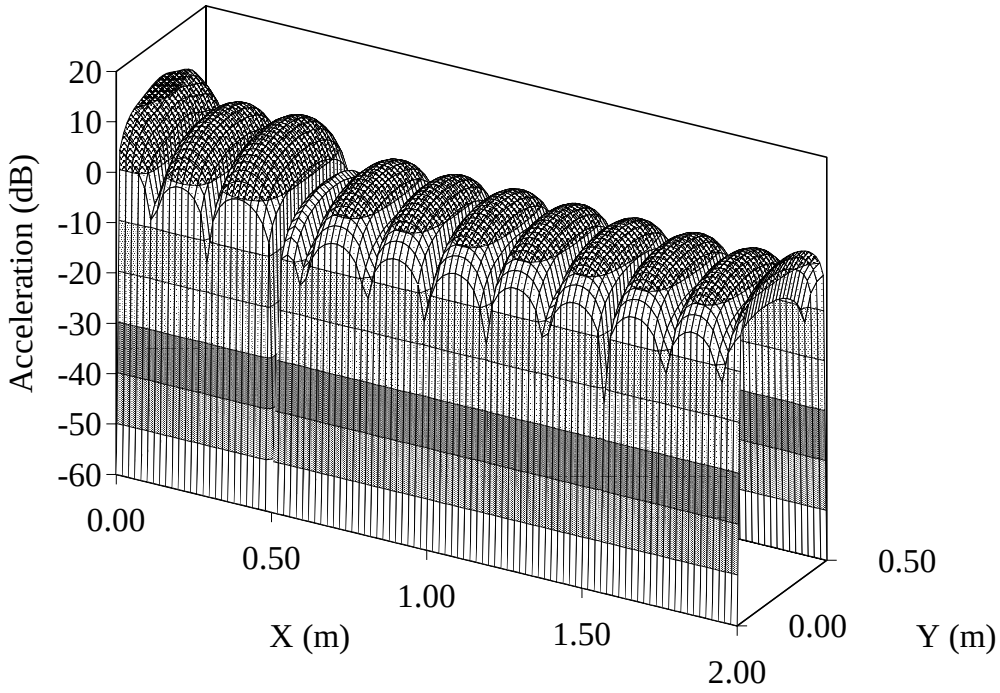

Figure 3.8 Uncontrolled finite plate acceleration distribution. Edges $y = 0$ and $y = 0.5$ are simply supported and the ends at $x = 0$ and $x = 2.0$ are free.

It can be seen from the nature of the response that the near field effects become insignificant at less than 0.2m (½ wavelength) from the plate ends and the stiffener location.

Figures 3.9 and 3.10 show the controlled acceleration amplitude distributions for the semi-infinite and finite plates with the three control sources driven by the same signal. The acceleration level is less downstream of the error sensor location than at the error sensor location (x_e = 1.0m). This is consistent with previous work dealing with minimisation of vibration at a line across a plate using control sources driven by the same signal (Pan and Hansen, 1994). The calculated reduction in acceleration amplitude downstream of the error sensor is over 30 dB for the semi-infinite plate and over 20 dB for the finite plate.

Figures 3.11 and 3.12 show the controlled acceleration amplitude distributions for the semi-infinite and finite plates with the three control sources driven independently. The acceleration level is at a minimum at the error sensor location (x_e = 1.0m). The calculated reduction in acceleration amplitude downstream of the error sensor is around 45 dB for the semi infinite plate and over 40 dB for the finite plate. The slope of the attenuation curve as a function of location in the *x*-direction is greater for the case with control sources driven independently. Independently driven control sources require less room to deliver a given level of attenuation than control sources driven by the same signal.

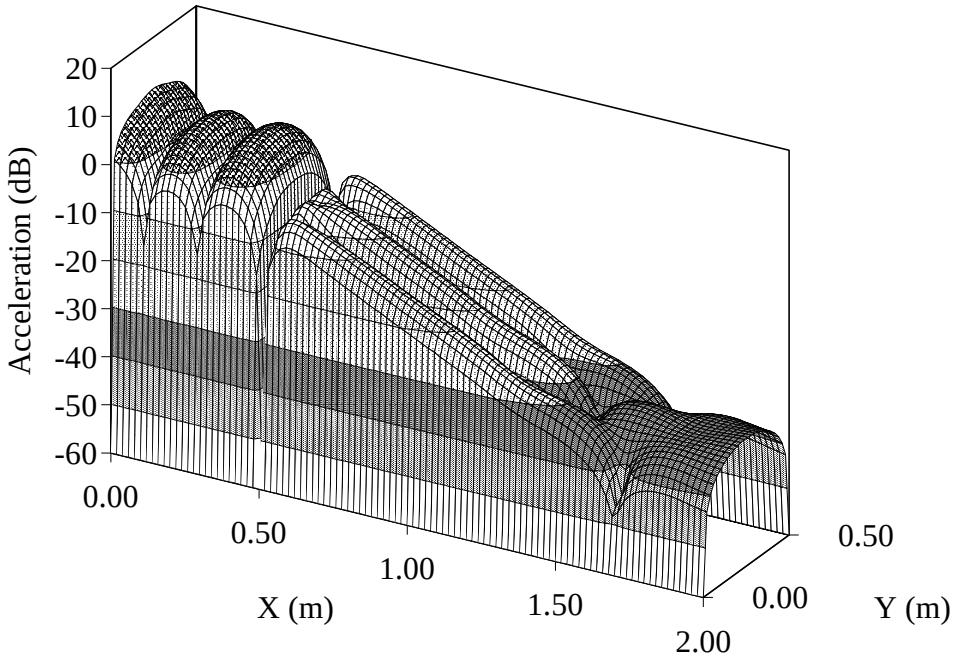

Figure 3.9 Controlled semi-infinite plate acceleration distribution - control sources driven by the same signal.

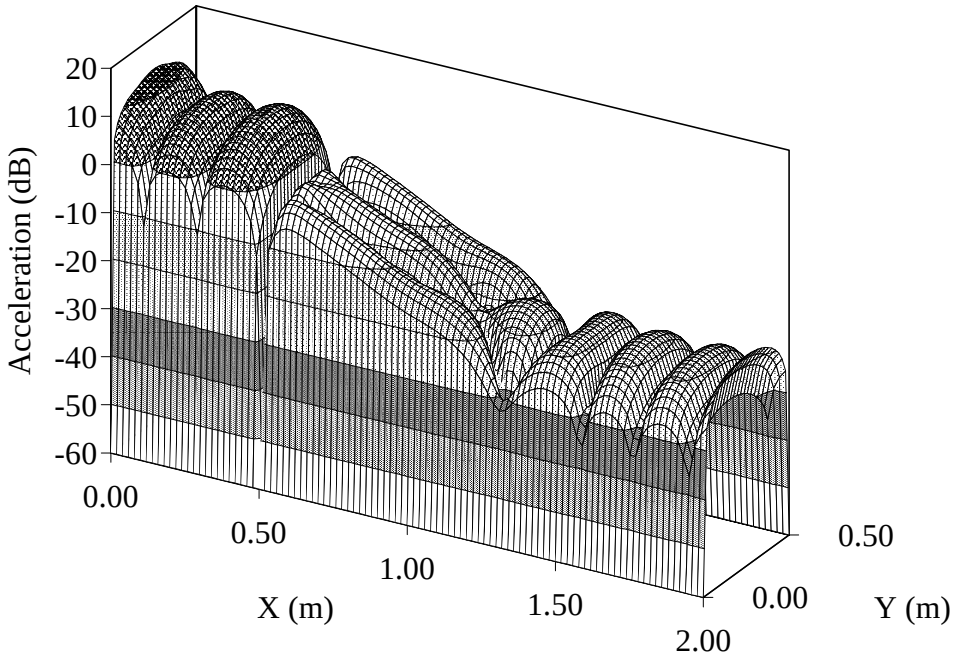

Figure 3.10 Controlled finite plate acceleration distribution - control sources driven by the same signal.

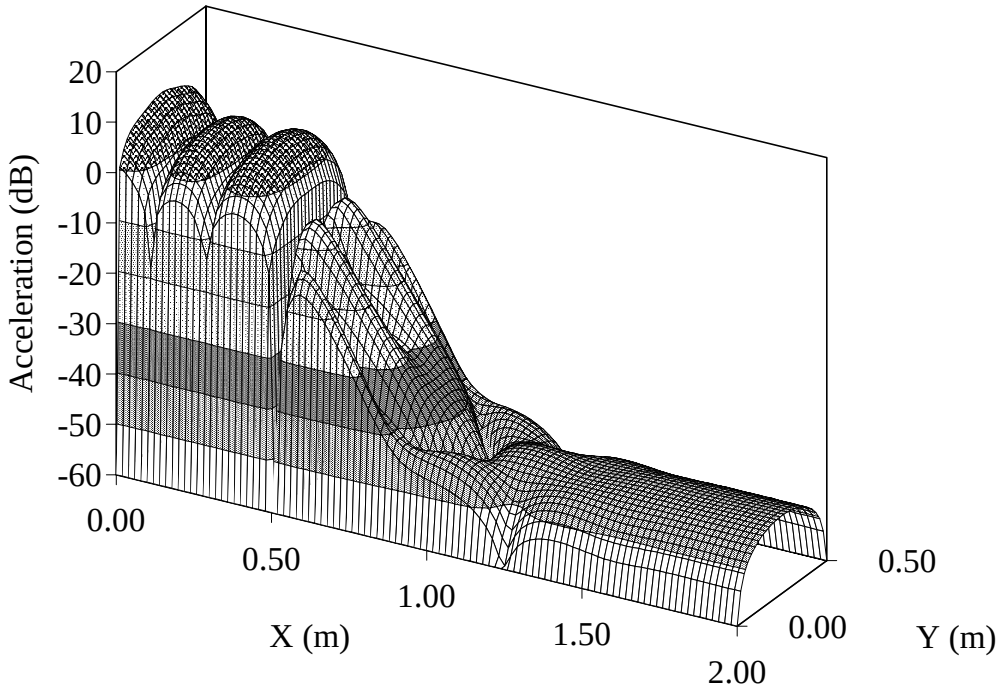

Figure 3.11 Controlled semi-infinite plate acceleration distribution - control sources driven independently.

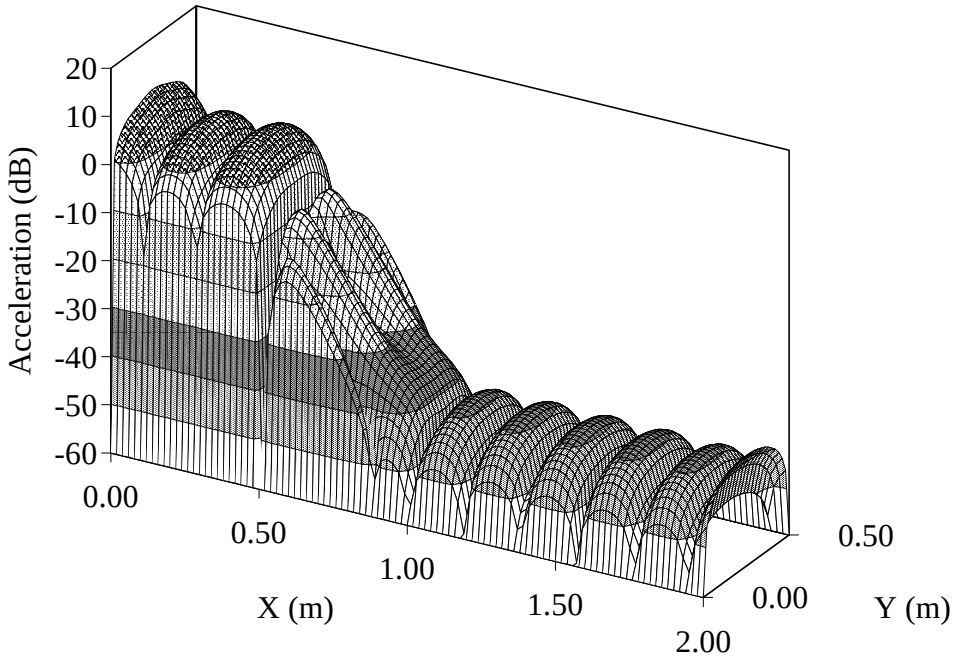

Figure 3.12 Controlled finite plate acceleration distribution - control sources driven independently.

3.3.2 Effect of variations in forcing frequency, control source location and error sensor location on the control forces

Figure 3.13 shows the effect of varying the forcing frequency on the magnitude of the control force(s). The average control force amplitude for the case where control sources are driven independently is generally slightly lower than the control force amplitude for the case when the control sources are driven by the same signal, as expected, because the energy input to the plate is more efficient with independently driven control sources. The independently driven control force amplitude is greater at some higher frequencies where control sources driven by the same signal do not control the vibration well. This will be discussed later.

The maxima at frequencies of 38 Hz, 96 Hz, 209 Hz and 380 Hz on Figure 3.13 occur when the relative spacing between primary and control sources is given by $x = (c + nx_s)$ for integer n and some constant c, where x_s is the spacing between axial nodes. This effect is illustrated by Figure 3.14 which shows the control force magnitude as a function of separation between primary and control sources, with a constant error sensor location - control source separation of 0.5 metres ($1.39\lambda_b$). The maxima occur because of the difficulty in controlling the flexural vibration when the control location corresponds to a node in the standing wave field developed by reflections from the free end and the stiffener. The constant c is frequency dependent and represents the distance (in wavelengths) between the primary source and the first node in the standing wave in the direction of the control source. The axial separation between nodes x_s is discussed further in Section 4.3.

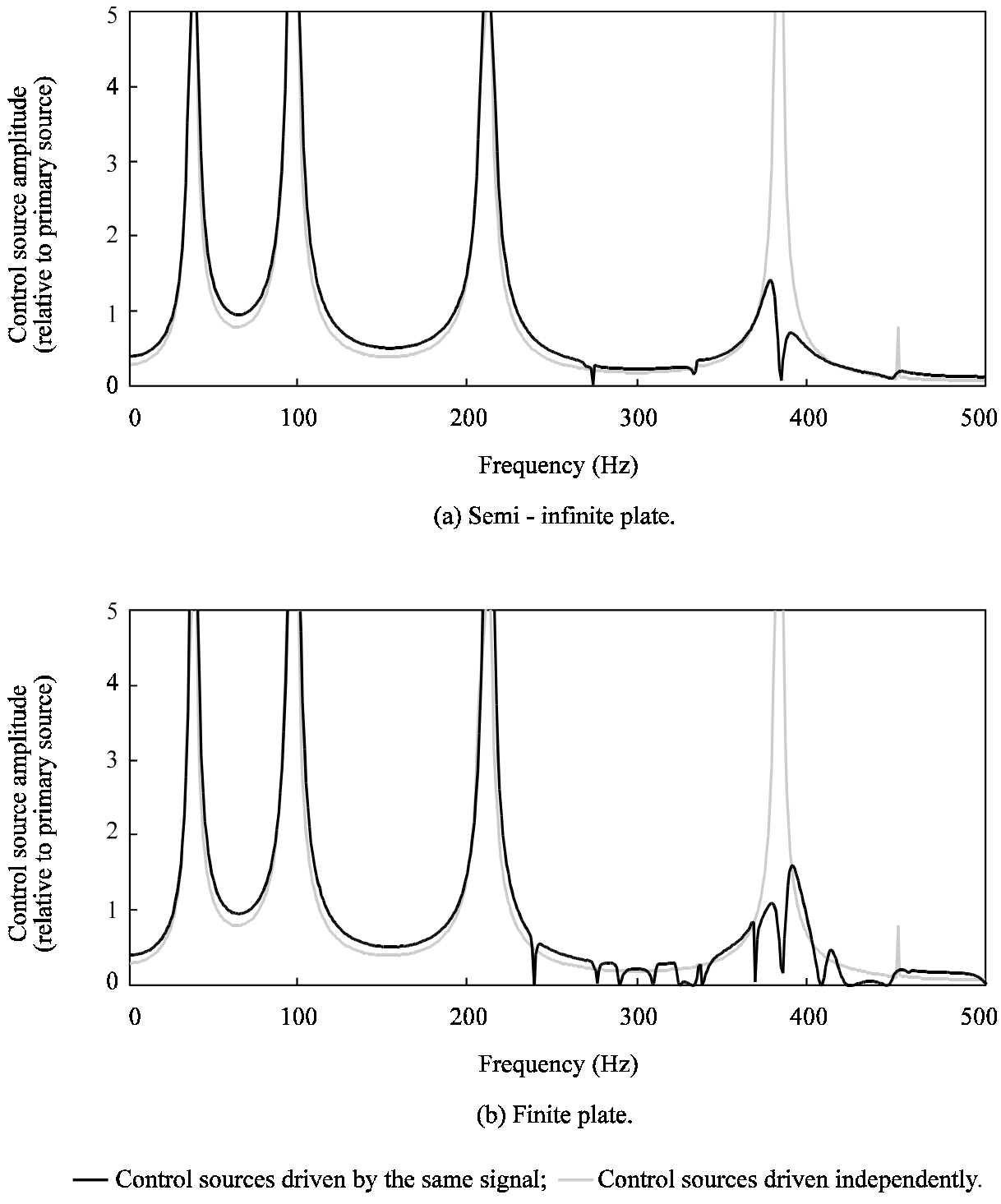

Figure 3.13 Mean control source amplitude for optimal control as a function of frequency. Three control sources and two primary sources were used.

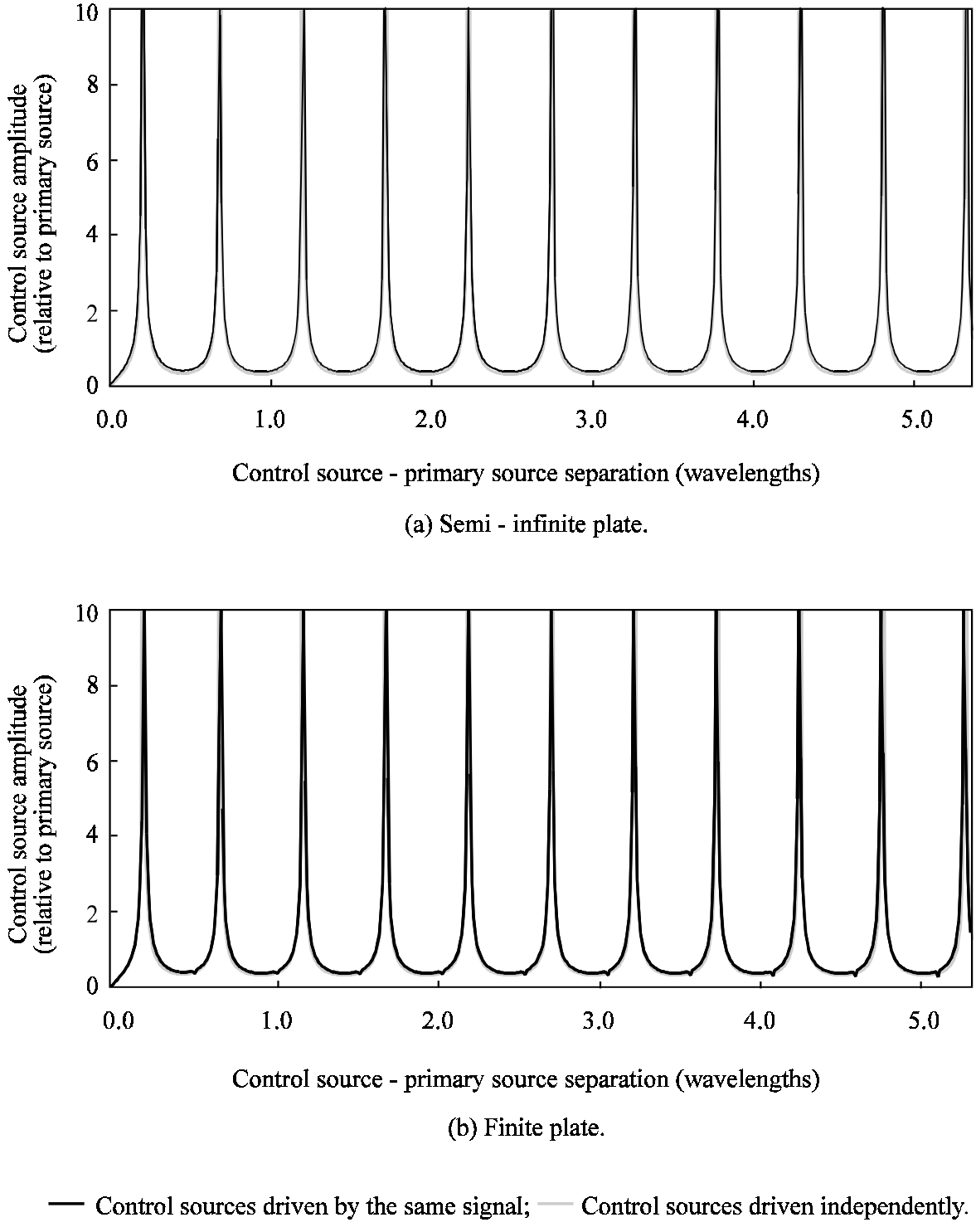

Figure 3.14 Mean control source amplitude for optimal control as a function of primary source - control source separation. Three control sources and two primary sources were used.

Figure 3.15 shows that the location of the line of error sensors does not significantly affect the control source amplitude, provided the error sensor location is outside of the control source near field.

The phase of the control source relative to the primary source is zero at all frequencies and for all locations of control source and error sensor, for independent control and for the case with control sources driven by a common signal. This result is due to the formation of the standing waves between the plate end(s) and stiffener location. When a standing wave is formed, the vibration, and hence the required control force, is in phase with the excitation.

3.3.3 Effect of variations in forcing frequency, control source location and error sensor location on the attenuation of acceleration level

Figure 3.16 shows the variation in the mean attenuation of acceleration level downstream of the error sensors as a function of frequency. For the semi-infinite plate, the main minima in the curve occur at the same frequencies as the maxima in the control source amplitude plot (Figure 3.13); that is, where the control location is at a node in the standing wave generated by waves reflected from the stiffener. This effect is not seen clearly in the plots for the finite plate, where reflections from the downstream end of the plate cause rapid variation in the achievable attenuation. For both plates, little attenuation is achieved with all of the control sources driven by the same signal above 280 Hz, which is the cut-on frequency for the second higher order cross-plate mode. Independently driven control sources can cope with the higher order cross-plate modes.

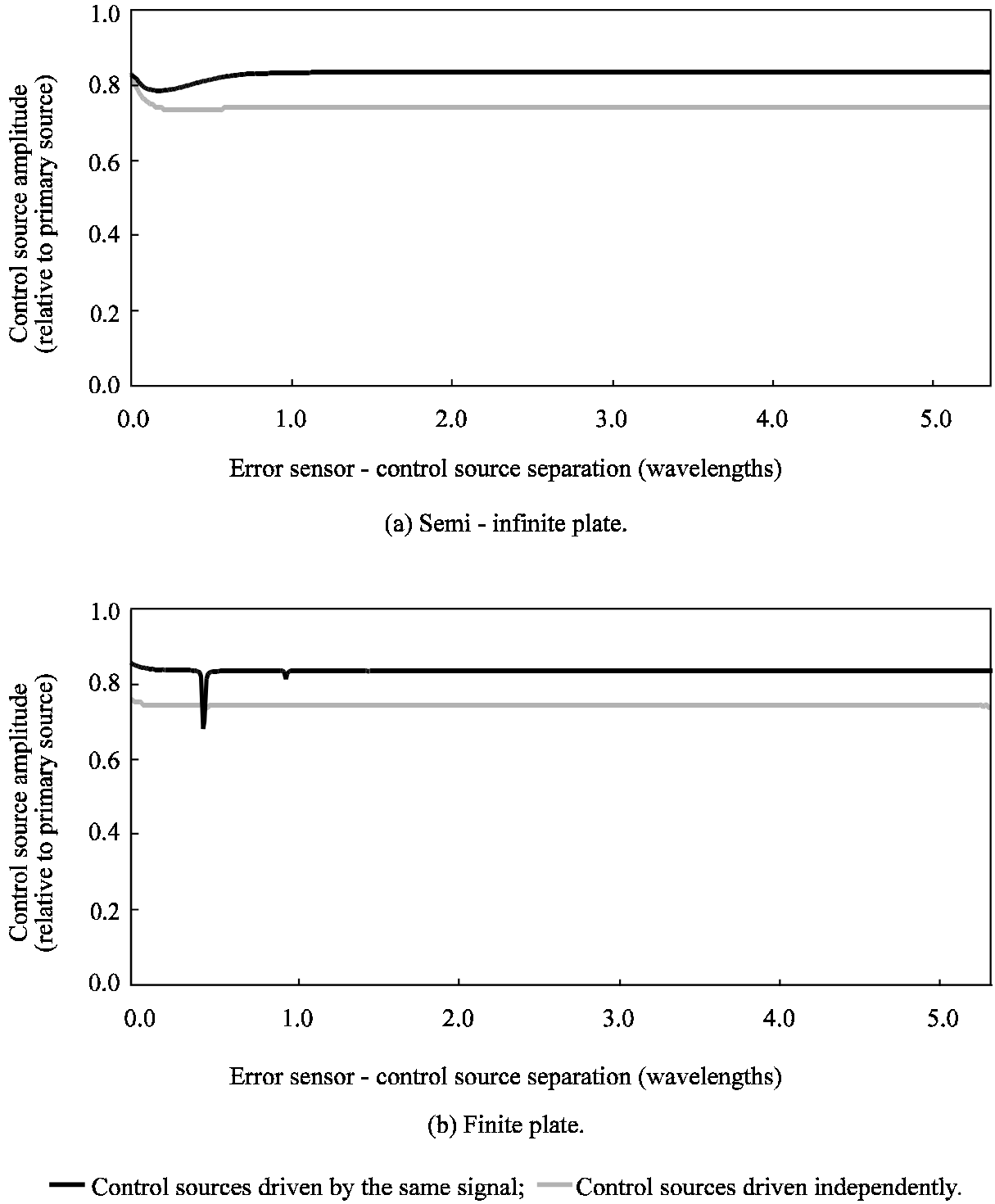

Figure 3.15 Mean control source amplitude for optimal control as a function of error sensor - control source separation. Three control sources and two primary sources were used.

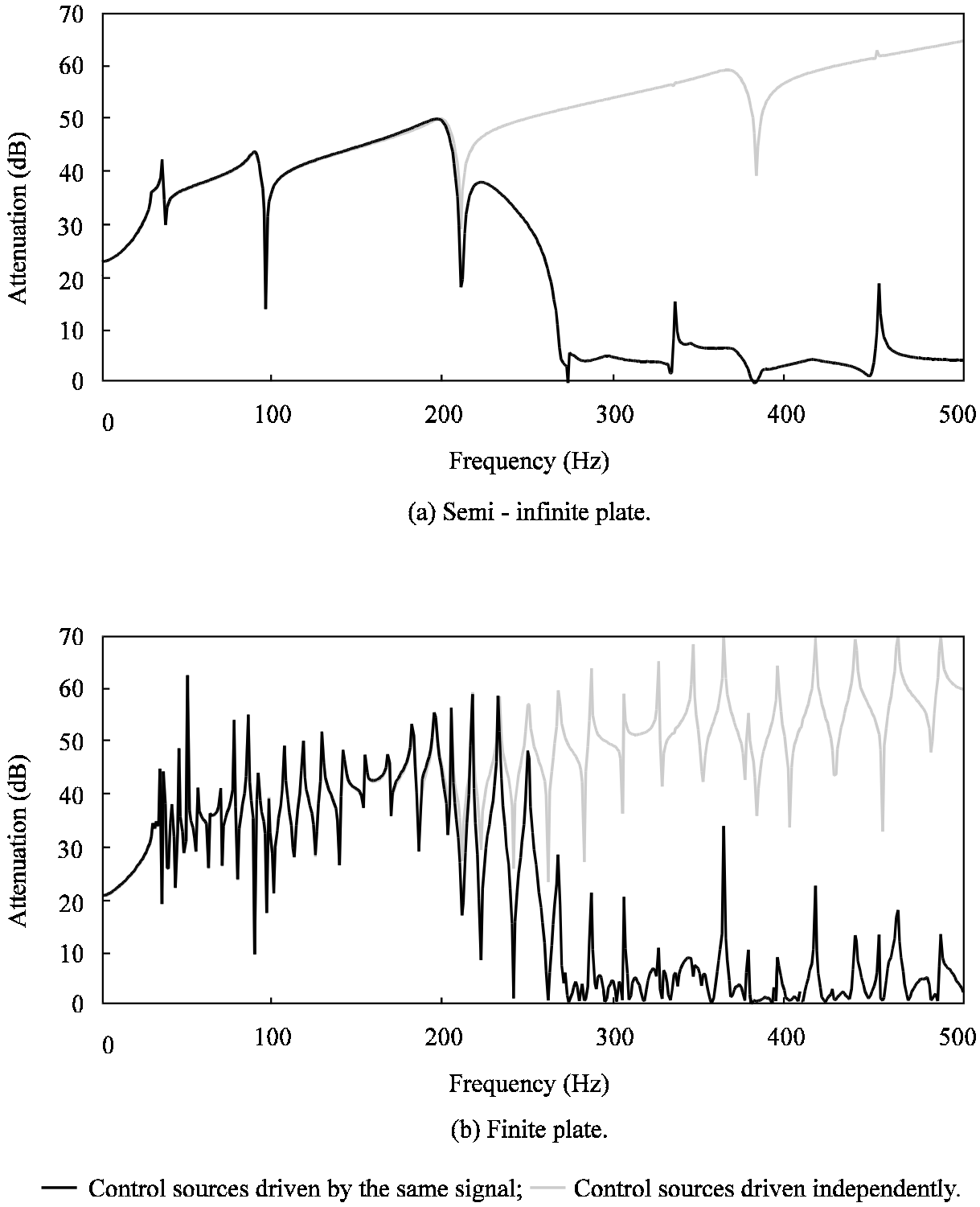

Figure 3.16 Mean attenuation downstream of the line of error sensors as a function of frequency.

The minima in the plot showing the variation in attenuation with separation distance between the primary and control sources on the semi-infinite plate (Figure 3.17(a)) correspond to maxima in the control source amplitude with control source location plot (Figure 3.14(a)), which occur as a result of the standing wave field set up between the stiffener and the upstream end of the plate. Similarly, every second minima in the plot for the finite plate (Figure 3.17(b)) corresponds to a maxima in Figure 3.14(b). The other minima in Figure 3.17(b) occur when the control location is at a node in the standing wave generated by reflections from the downstream plate end.

Figure 3.18 shows the mean attenuation downstream of the error sensor as a function of the separation between the control source and the line of error sensors. For the cases where the control sources are driven by a common signal, attenuation increases with increasing separation between the line of error sensors and the control location at the rate of about 18 dB per wavelength separation, up to a maximum of about 85 dB above four wavelengths separation. The achievable attenuation increases with greater separation between the control sources and the error sensors because the near field component of the control excitation diminishes with greater separation. The maximum is limited by the accuracy of the calculations. The maximum attenuation achievable experimentally would of course be lower. When the control sources are driven independently, the slope of the attenuation curve is greater.

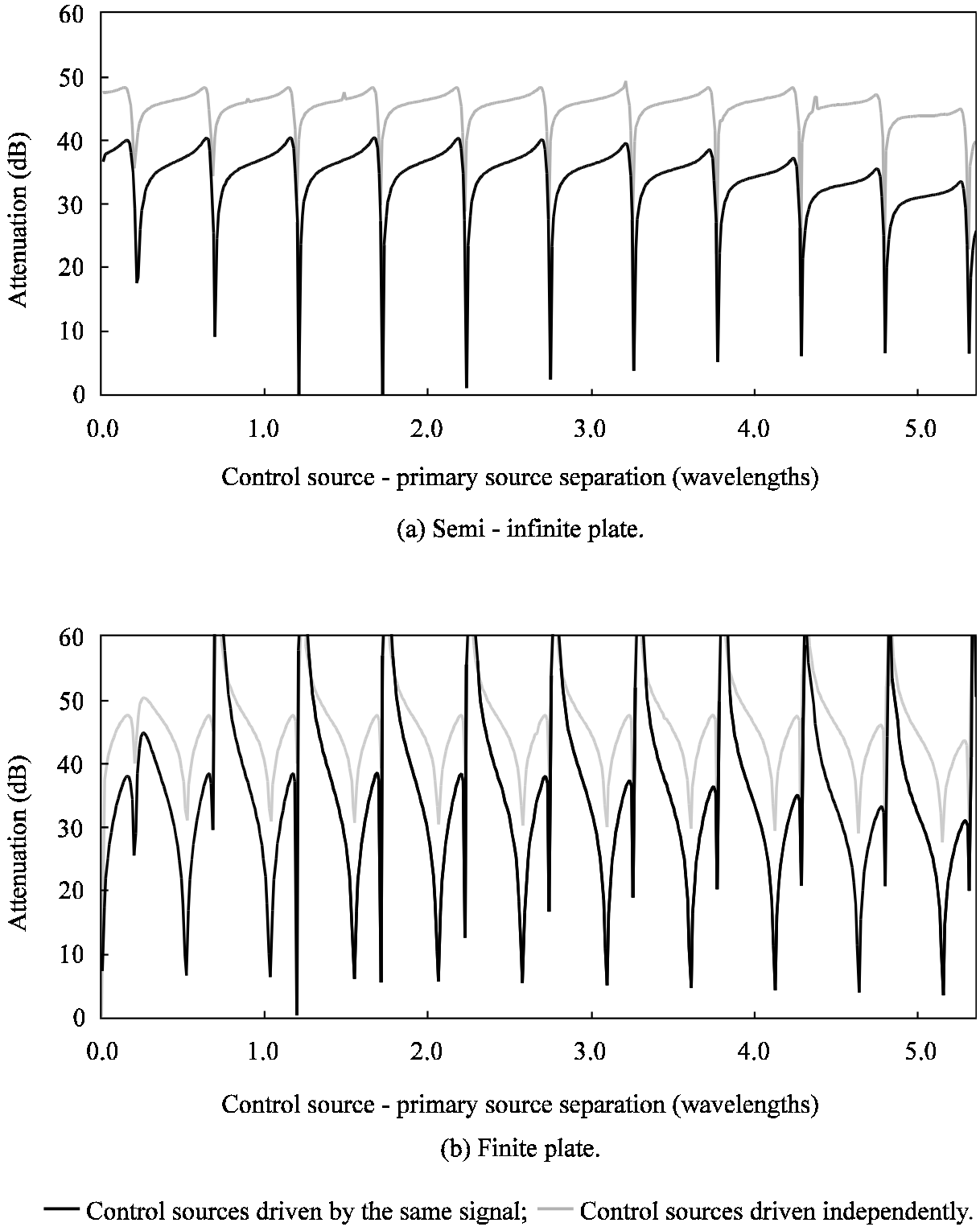

Figure 3.17 Mean attenuation downstream of the line of error sensors as a function of control source - primary source separation.

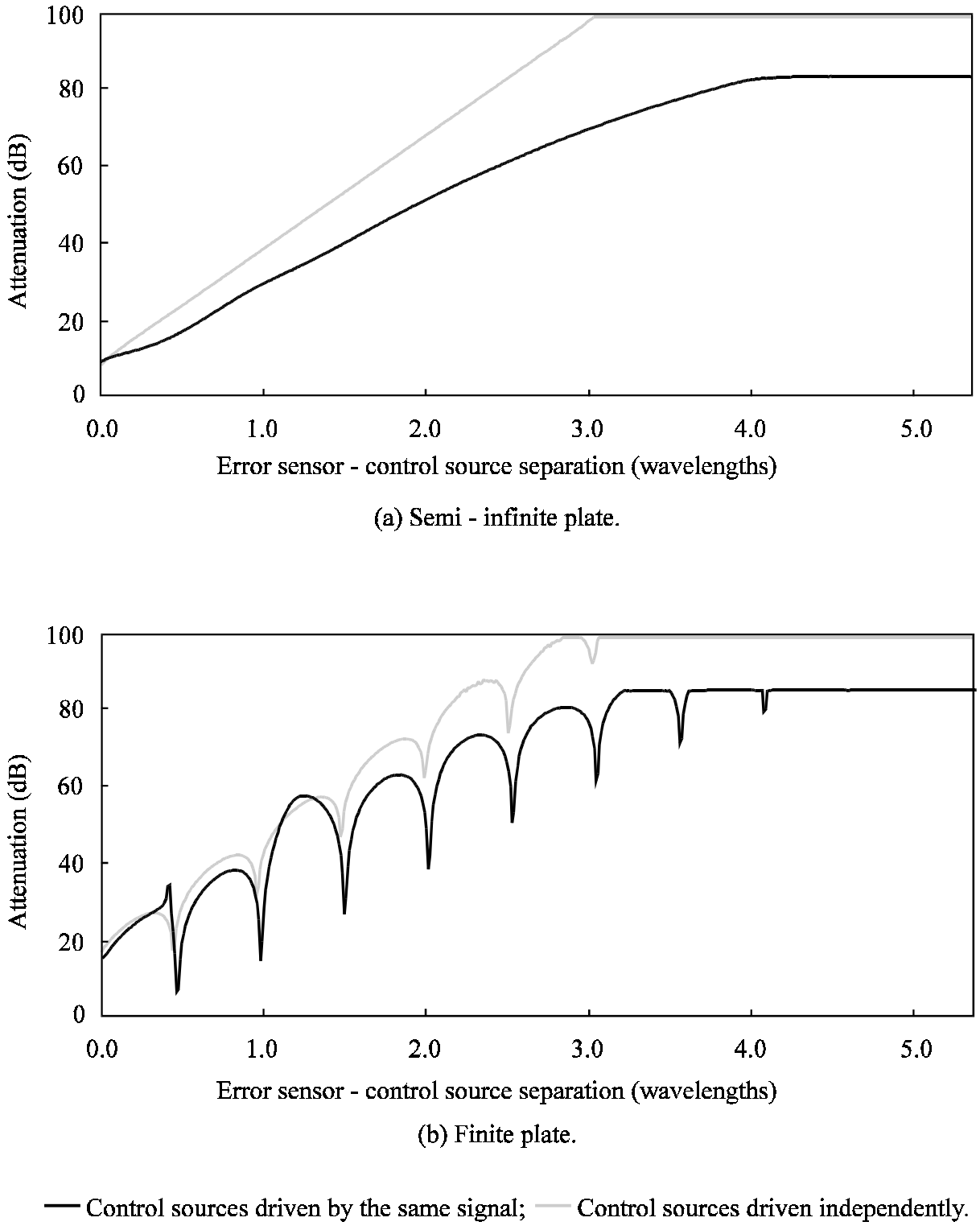

Figure 3.18 Mean attenuation downstream of the line of error sensors as a function of error sensor - control source separation.

3.3.4 Number of control sources required for optimal control

Table 3.2 shows the amount of attenuation of acceleration level achieved downstream of the error sensors with various numbers of control sources. The control sources are located at a single axial location. The across-plate locations are given by $y_{c1} = 0.08$, $y_{c2} = 0.25$, $y_{c3} = 0.33$, $y_{c4} = 0.40$, and $y_{c5} = 0.42$. The other locations of primary sources, control sources and error sensors and the plate dimensions used were those given in Table 3.1. The results given are for the semi-infinite plate.

Table 3.2

Effect of the Number of Control Sources on Mean Attenuation

Number of Control Sources	Mean Attenuation (dB)
1	4.54
2	28.2
3	44.4
4	44.4
5	44.4

3.3.5 Effect of a second angle stiffener and set of control sources on the attenuation of acceleration level

The results given in Section 3.3.3 indicate that there are some control source locations where significantly less attenuation can be achieved. Figure 3.19 shows the variation in mean control source amplitude using six control sources located in two sets of three, driven to optimally

control vibration at a single line of error sensors, as a function of control source location. The control source signals are calculated by the method described in Section 3.2.5.3. The second angle stiffener and set of control sources is located 0.15m downstream from the first, and the line of error sensors is located 0.5m downstream from the first control source. The mean control source amplitude using a single set of control sources is also shown in Figure 3.19 for comparison. Figure 3.20 shows the mean attenuation of acceleration level downstream of the line of error sensors as a function of control location, using one and two sets of control sources. At this frequency, there are no control source locations at which control using the two sets of control sources is difficult. Figure 3.20 shows that good control can be achieved at any frequency using two sets of control actuators.

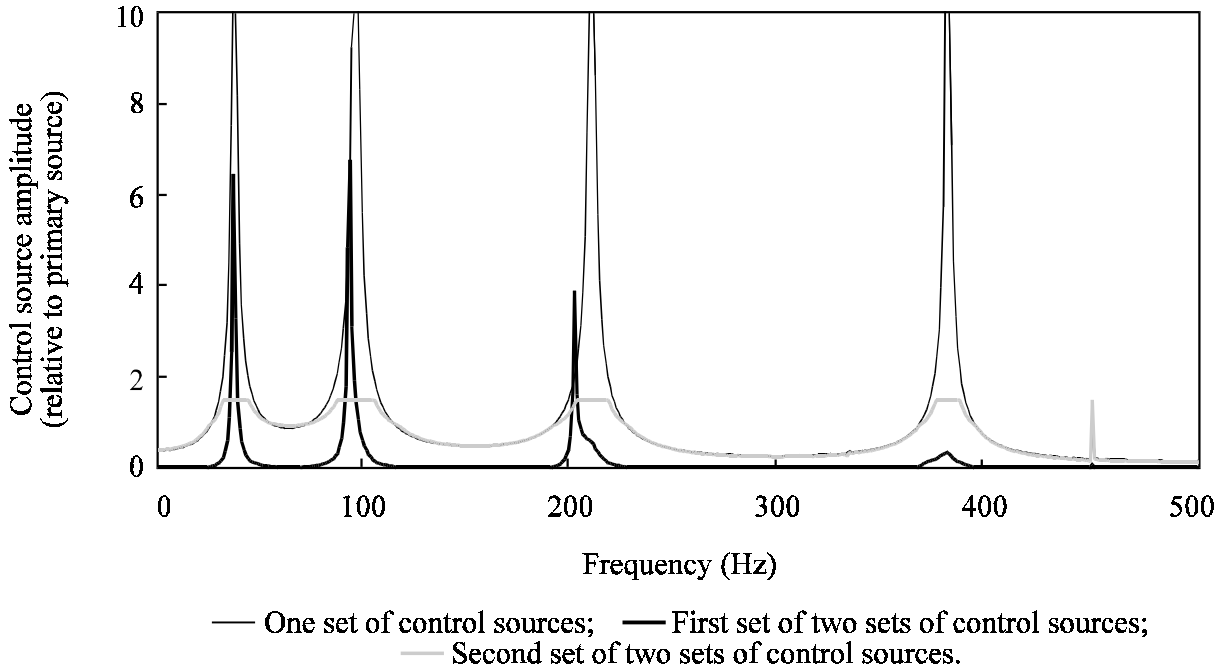

Figure 3.19 Mean control source amplitude for optimal control using one and two sets of independently driven control sources as a function of frequency for the semi-infinite plate.

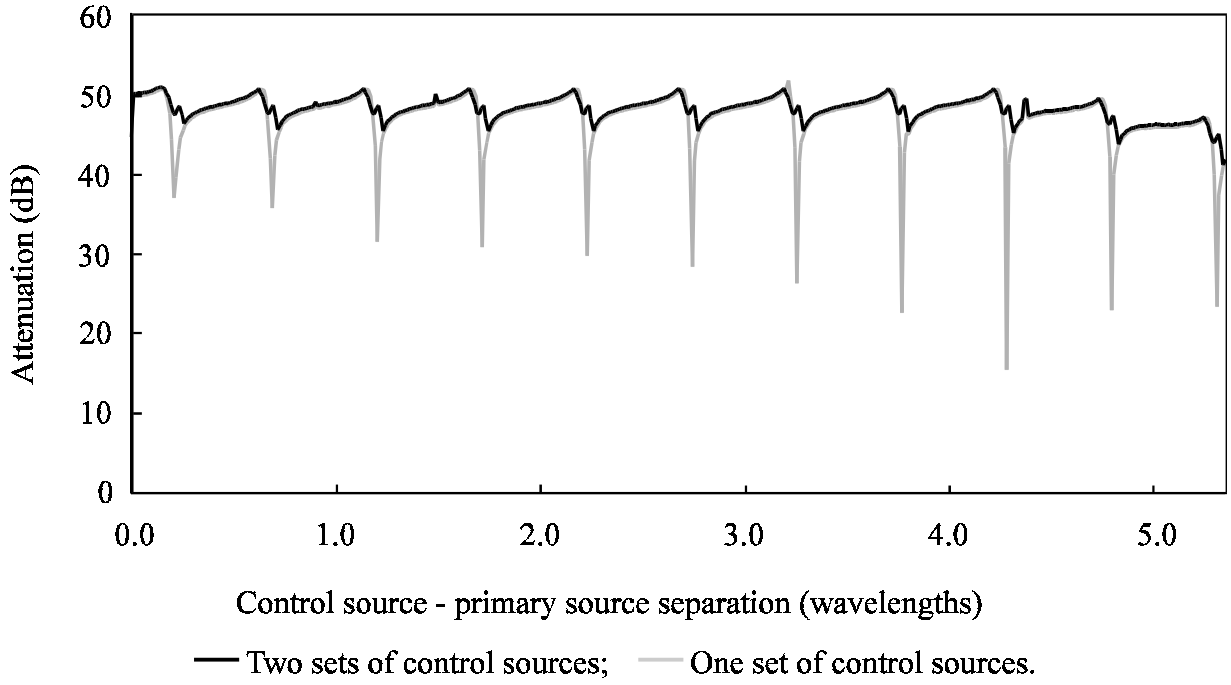

Figure 3.20 Mean attenuation downstream of the line of error sensors using one and two sets of independently driven control sources as a function of control source -primary source separation for the semi-infinite plate.

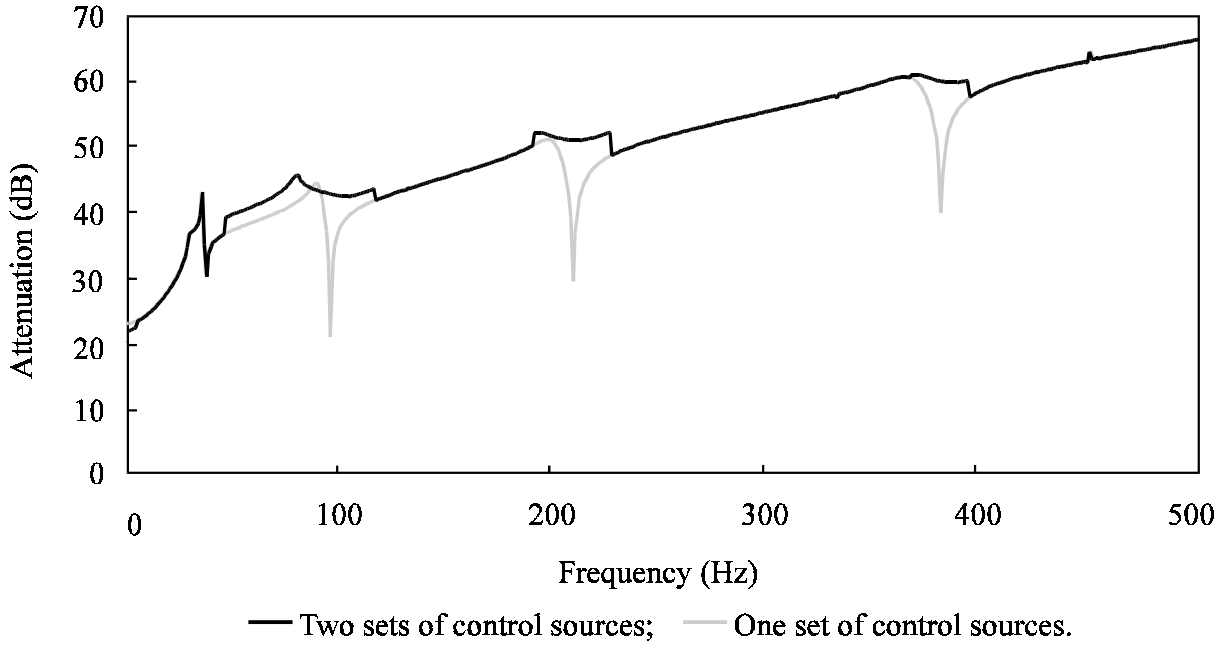

Figure 3.21 Mean attenuation downstream of the line of error sensors using one and two sets of independently driven control sources as a function of frequency for the semi-infinite plate.

3.3.6 Number of error sensors required for optimal control

Table 3.3 shows the control source amplitude and amount of attenuation of acceleration level achieved downstream of the error sensors with various numbers of error sensors. The error sensors were located at axial location x_e = 1.0m and unevenly spaced across-plate locations. The other locations of primary sources and control sources and the plate dimensions used were those given in Table 3.1. The results given are for the semi-infinite plate.

Table 3.3

Effect of the Number of Error Sensors on Control Source Amplitude and Mean Attenuation

Number of Error Sensors	Mean Control Source Amplitude*	Mean Attenuation (dB)
1	0.83446	0.24127
2	1.5046	6.6589
3	0.74635	44.306
4	0.74636	44.329
5	0.74636	44.307
6	0.74636	44.372
7	0.74636	44.401
8	0.74636	44.467
9	0.74635	44.527
10	0.74635	44.576
∞	0.74635	44.626

*Mean control source amplitude is expressed relative to the primary source amplitude. Three control sources and two primary sources were used.

3.4 EXPERIMENTAL PROCEDURE

3.4.1 Modal analysis

A modal analysis was performed on the plate to be used in the vibration control experiment. The software package "PC Modal" was used to perform the analysis. The modal analysis experimental arrangement is given in Figure 3.22. A Brüel and Kjær type 8202 impact hammer and type 2032 signal analyser were used in the modal analysis. The dimensions of the plate were the same as those given in Section 3.3 (see Table 3.1). The plate model consisted of 96 nodes dividing the plate into 10cm squares. The analysis was performed for the two cases with and without the angle stiffener attached to the plate.

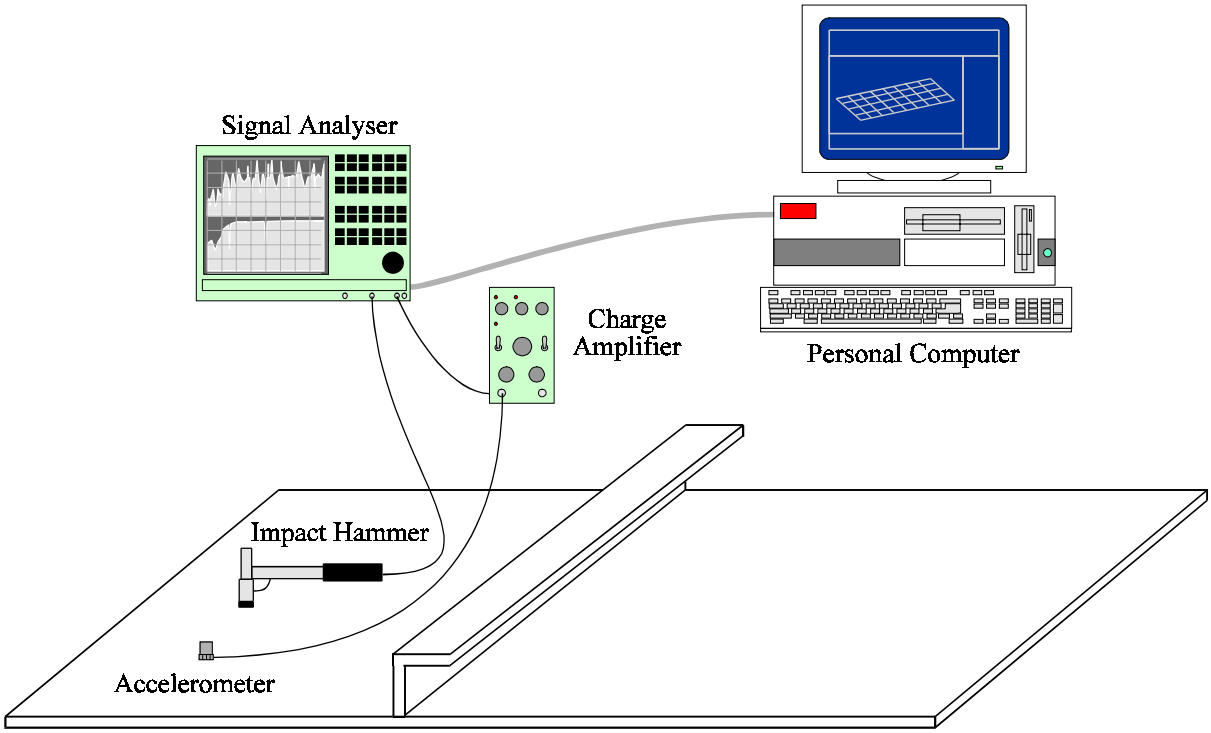

Figure 3.22 Experimental arrangement for the modal analysis of the plate.

3.4.2 Active vibration control

A steel stiffener was bolted tightly to a plate of the same dimensions described in the Section 3.3 (see Table 3.1). Three piezoceramic actuators were placed between the stiffener flange and the plate. The actuators were attached only at one end to ensure that no external tensile force were applied to them, as the type of actuator used is weak in tension. The primary source, control source and error sensor locations and the excitation frequency are also given in Table 3.1. The plate was mounted horizontally and excited in the vertical plane.

The complete experimental arrangement is given in Figure 3.23. The experimental equipment can be divided into three functional groups; the primary excitation system, the control system and the acceleration measurement system.

The primary signal was produced by a signal analyser and amplified to drive the electrodynamic shakers (Figure 3.24). The shakers acted on the plate through force transducers, and the magnitudes of the primary forces were recorded using an oscilloscope.

The error signals from the line of six accelerometers (Figure 3.25) were passed to a transputer controller. The controller determined the control signals to drive the piezoceramic actuators, optimally minimising the acceleration measured by the error sensors. The control signals were also recorded on an oscilloscope.

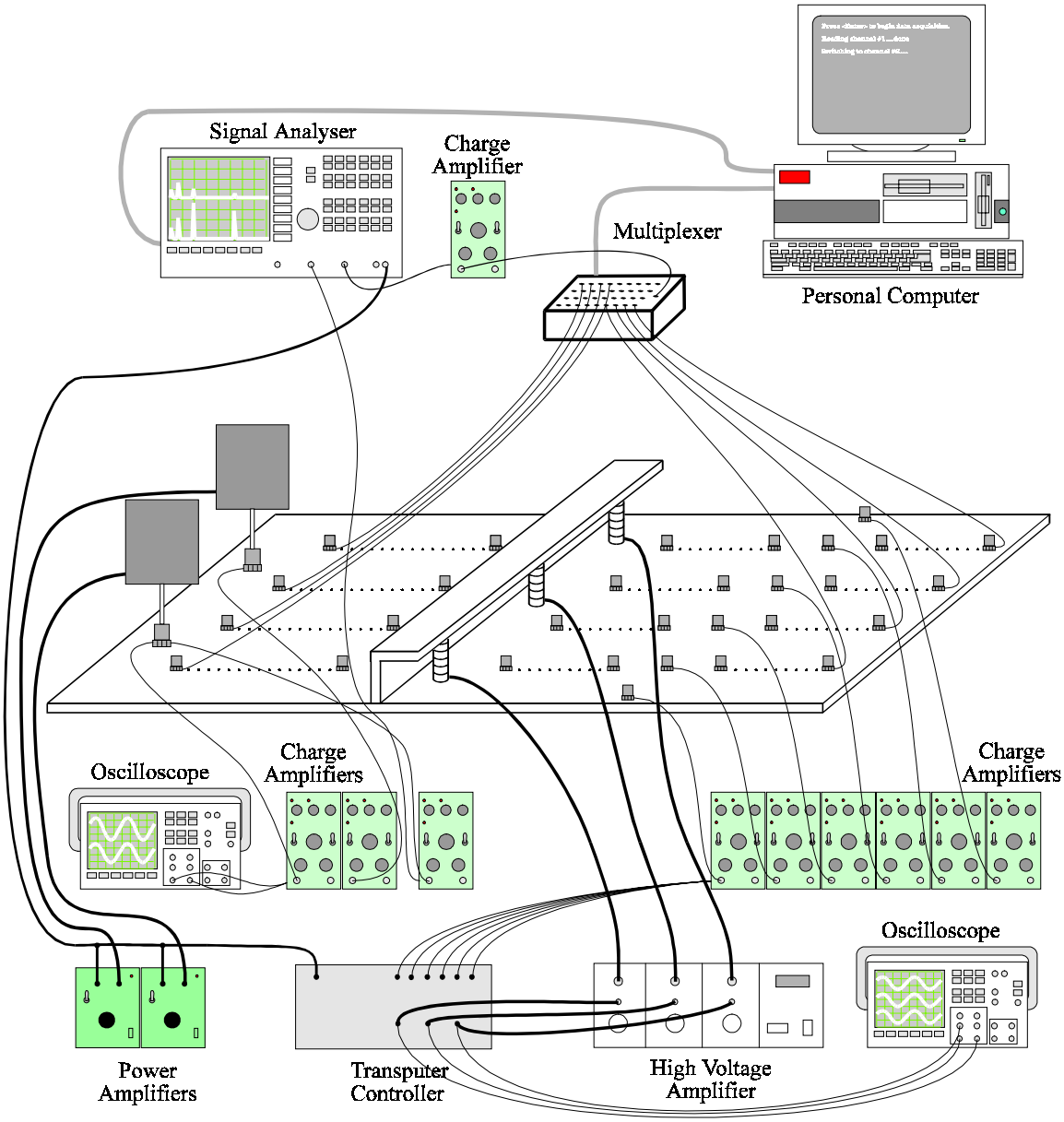

Figure 3.23 Experimental arrangement for the active control of vibration in the plate.

The acceleration was measured at 10 or 15 cm intervals along the plate in four lines equally spaced across the plate (Figure 3.26). The accelerometer signals were read in turn through a 40 channel multiplexer connected to a Hewlett-Packard type 35665A signal analyser. The frequency

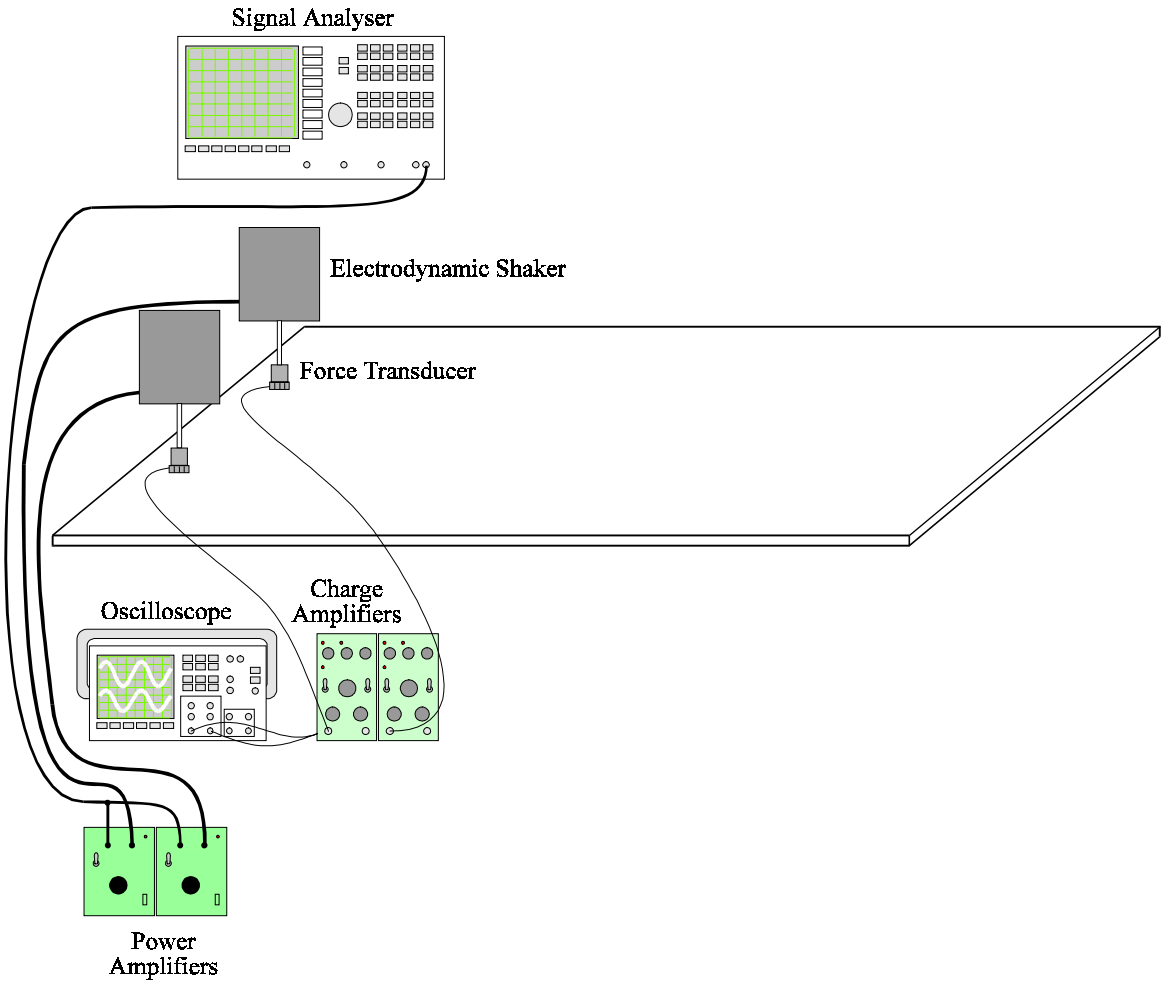

Figure 3.24 Primary system.

response function was used to analyse the data. The magnitude and phase of the acceleration were recorded on a personal computer, which was also used to switch the recorded channel on the multiplexer. The acceleration output of the force transducer at one of the primary locations was used as the reference signal for the frequency response analysis. Accelerometer readings were taken initially once the error sensor signals had been optimally reduced, and again with the control amplifiers switched off (the uncontrolled case). The experiment was repeated with the three control actuators driven by a common control signal.

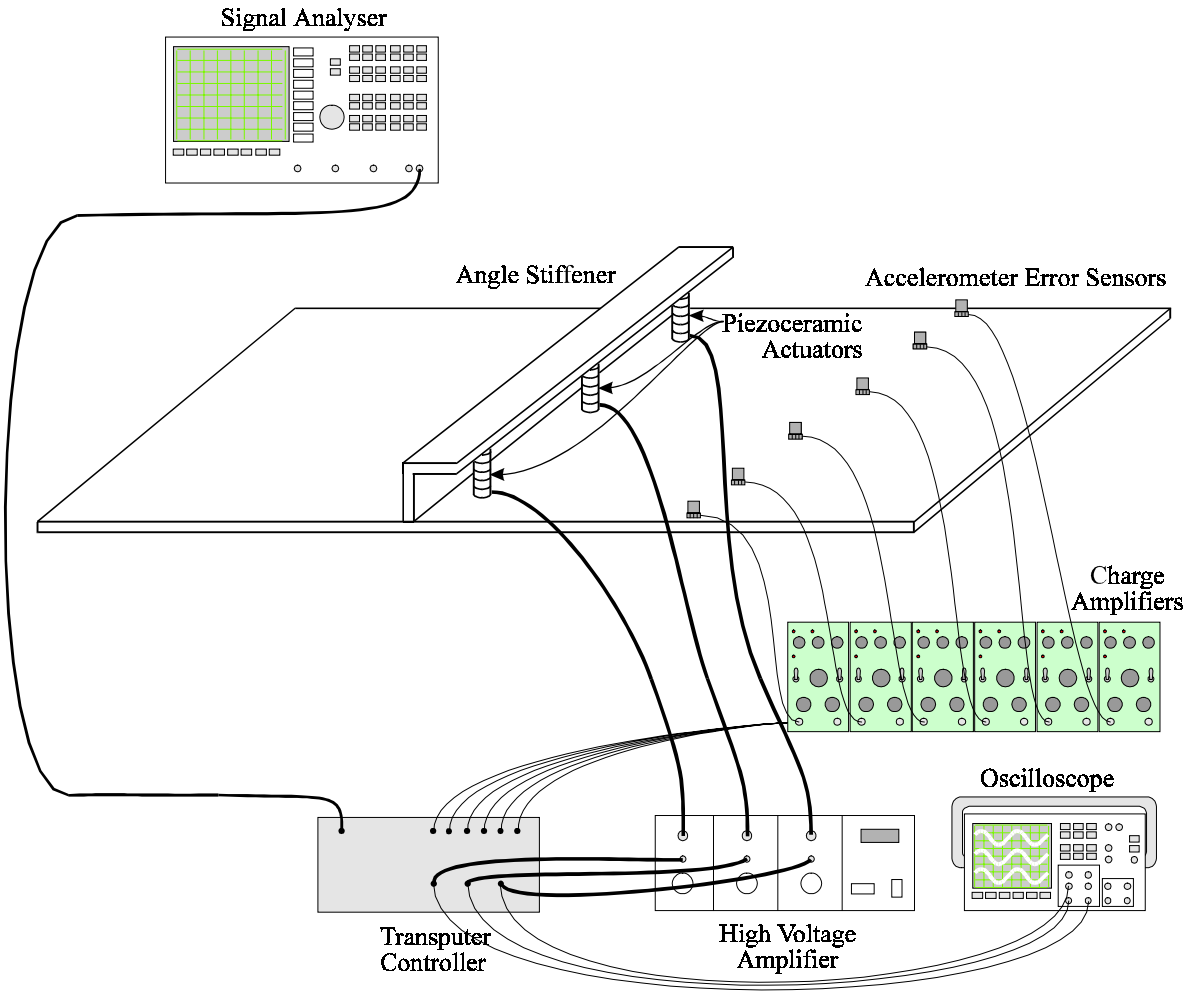

Figure 3.25 Control system.

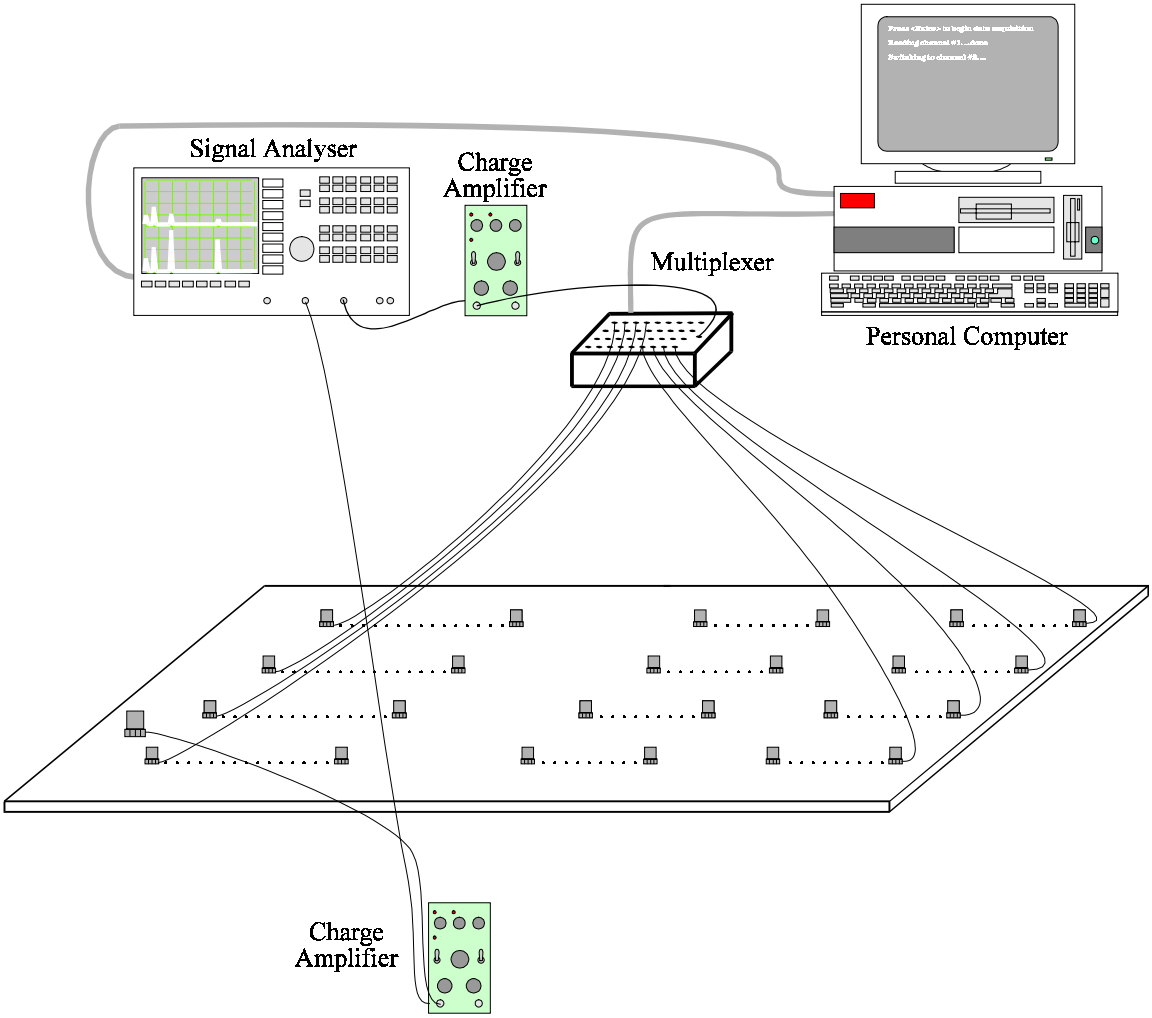

Figure 3.26 Acceleration measurement. Not all of the accelerometer - multiplexer connections are shown.

Figures 3.27 - 3.29 show the photographs of the experimental equipment. In Figure 3.27, the plate can be seen in the foreground with the signal generating and recording equipment in the background. The plate is simply supported along the two long edges and the far end is mounted in a diverging sandbox termination, approximating a semi-infinite end. The near end is free. Two electromagnetic shaker primary sources can be seen, as well as the angle stiffener mounted across the plate and accelerometers mounted at various positions on the plate. The plate is shown closer-up in Figure 3.28, with the primary sources removed. The piezoceramic stack actuators are shown in Figure 3.29, mounted between the stiffener flange and the plate surface.

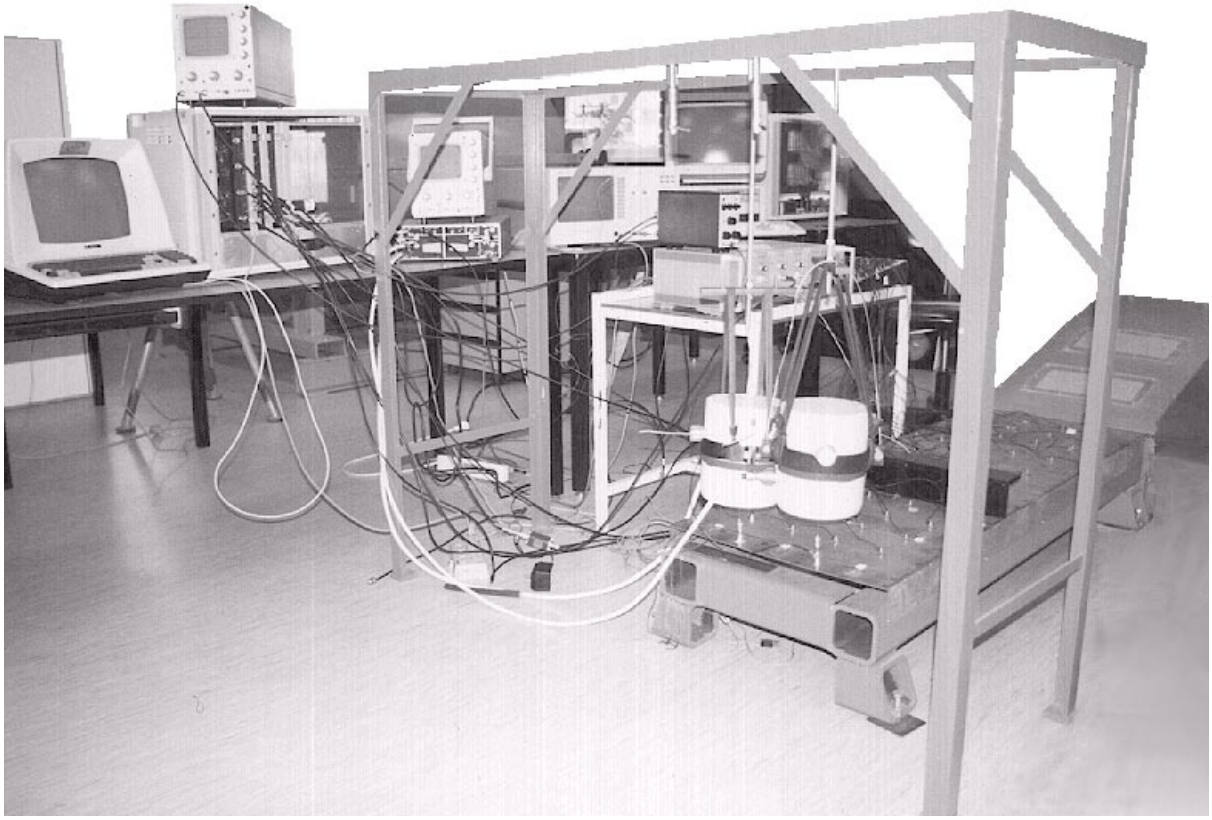

Figure 3.27 Experimental equipment for the active vibration control of plate vibration.

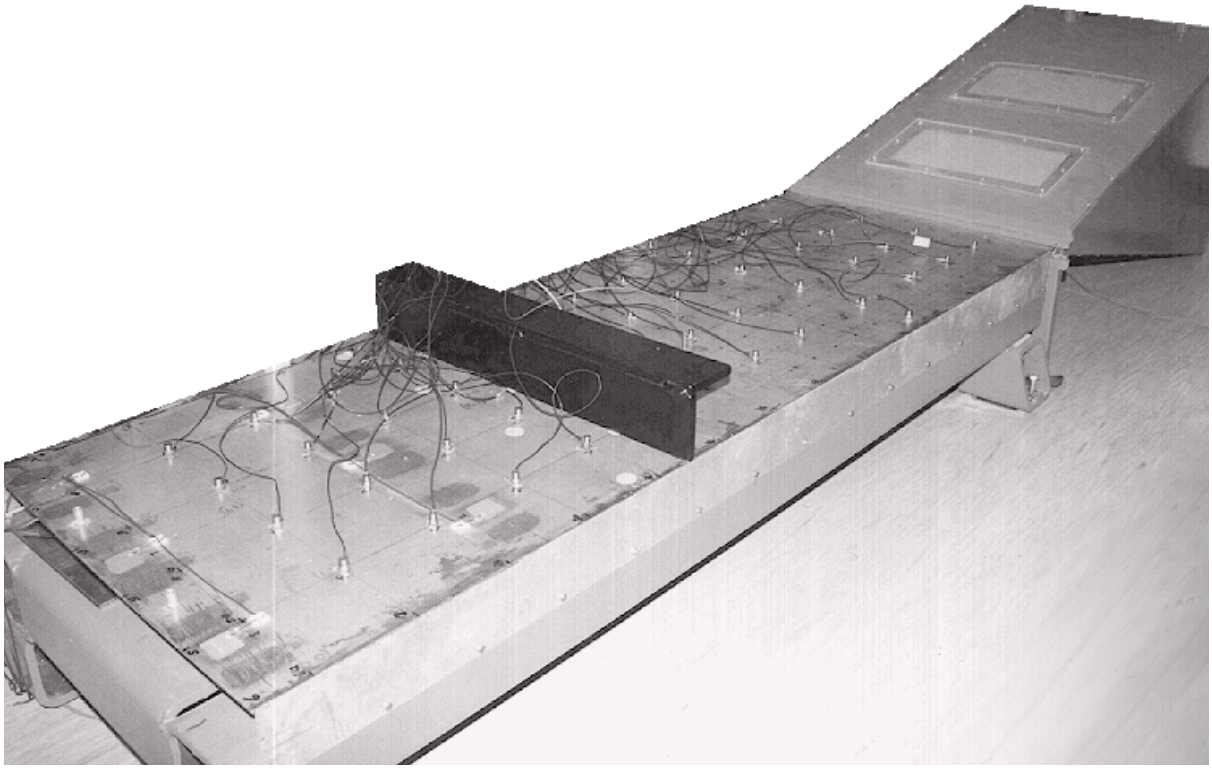

Figure 3.28 Accelerometers and angle stiffener mounted on the plate.

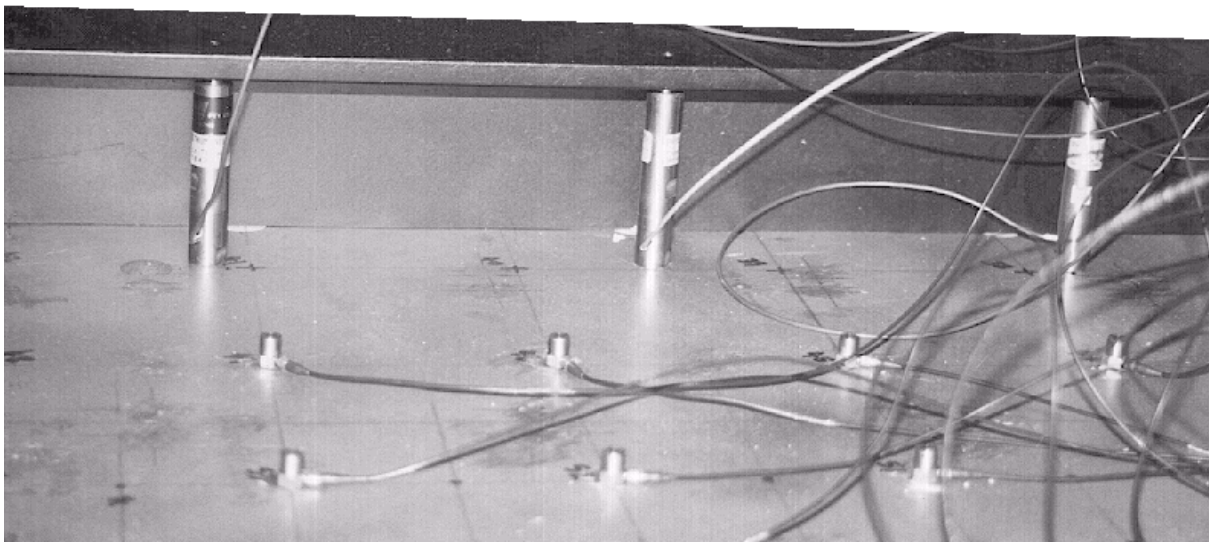

Figure 3.29 Piezoceramic stack actuators mounted between the plate and the flange of the angle stiffener.

3.5 EXPERIMENTAL RESULTS

3.5.1 Modal analysis

Figures 3.30 - 3.33 show the differences between the vibration response of the plate with and without the angle stiffener attached for the *n*,1 modes (*n* = 1,4). The presence of the angle stiffener makes a significant difference to the mode shapes.

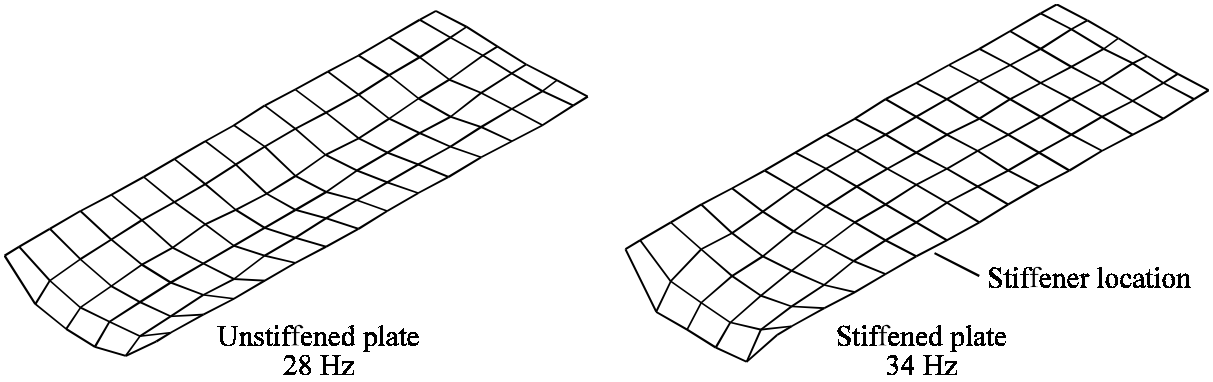

Figure 3.30 The 1,1 mode for the unstiffened and stiffened plate.

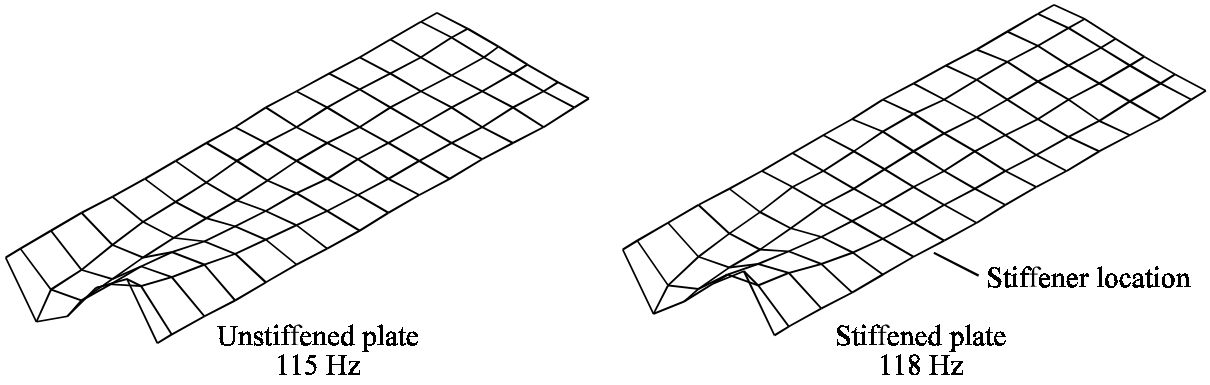

Figure 3.31 The 2,1 mode for the unstiffened and stiffened plate.

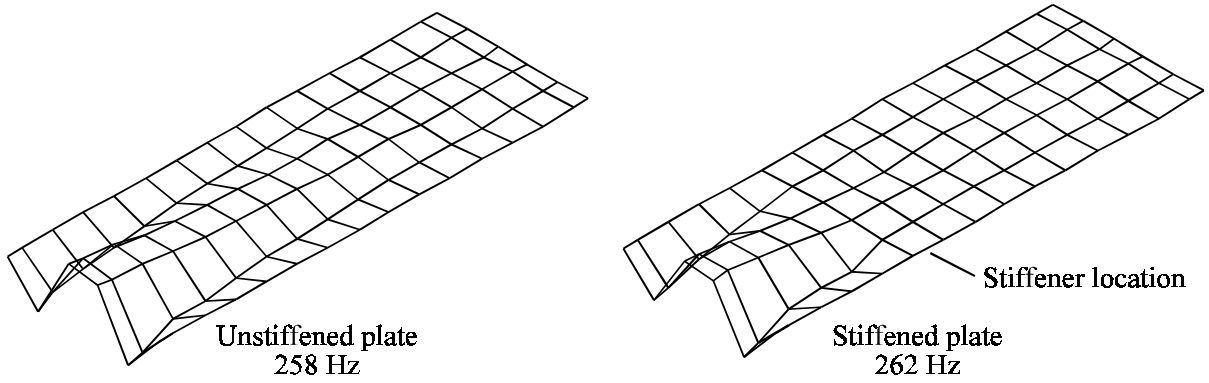

Figure 3.32 The 3,1 mode for the unstiffened and stiffened plate.

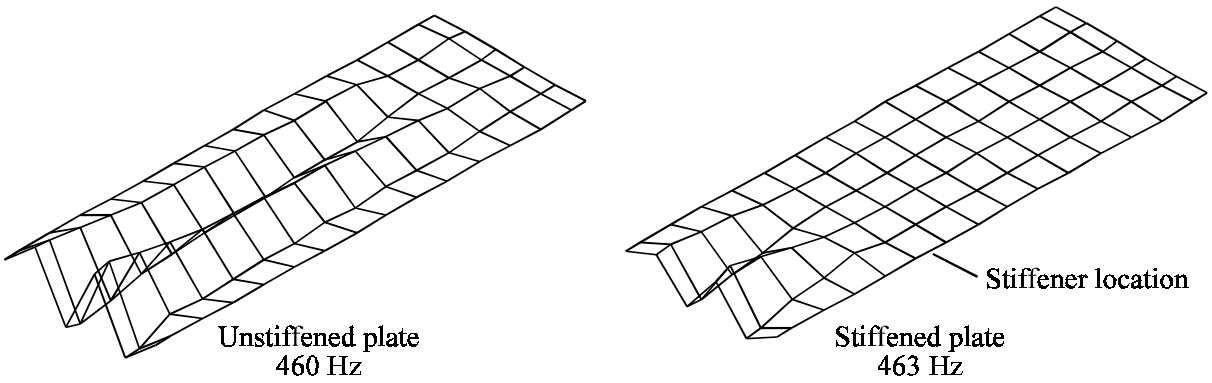

Figure 3.33 The 4,1 mode for the unstiffened and stiffened plate.

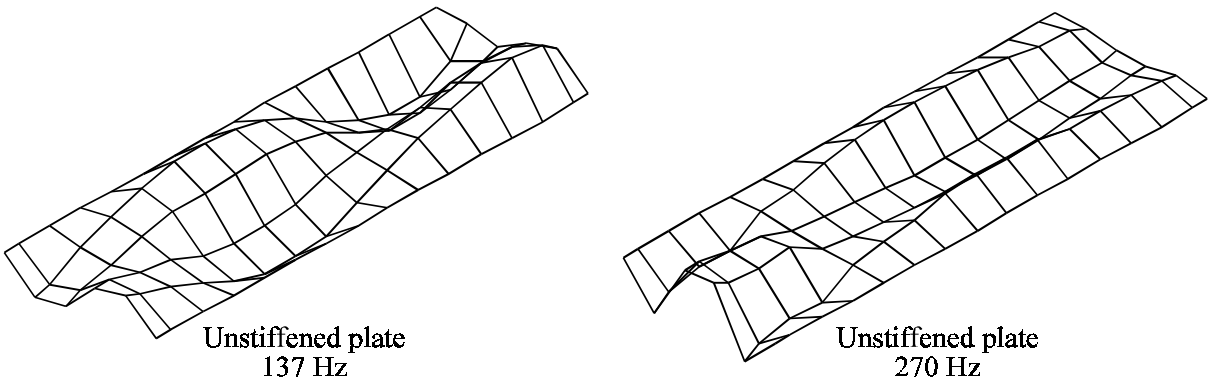

Figure 3.34 The 2,3 and 3,2 modes for the unstiffened plate.

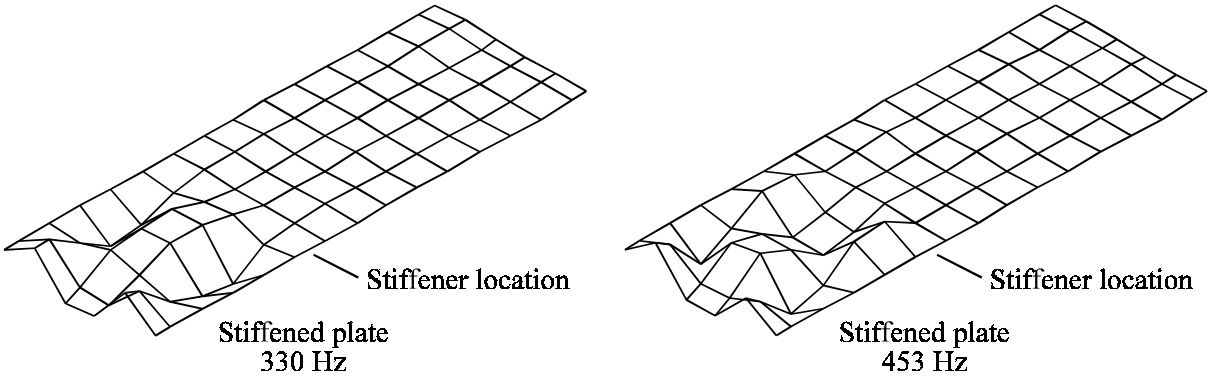

Figure 3.35 The 3,2 and 3,3 modes for the stiffened plate.

3.5.2 Active vibration control

Figure 3.36 shows the theoretical and experimental acceleration distributions for each of the four lines where accelerometers were placed in the experiment for the semi-infinite plate. For both the uncontrolled case and the controlled case with control actuators driven by the same signal, the experimental results and theoretical curves are in close agreement. For the controlled case with three independently driven control sources, the theoretical analysis predicted greater reduction in acceleration level than was achieved experimentally. An error analysis showed that a very small error (a tenth of a percent) in the control signal would produce a decrease in attenuation corresponding to the difference between the experimental and theoretical data.

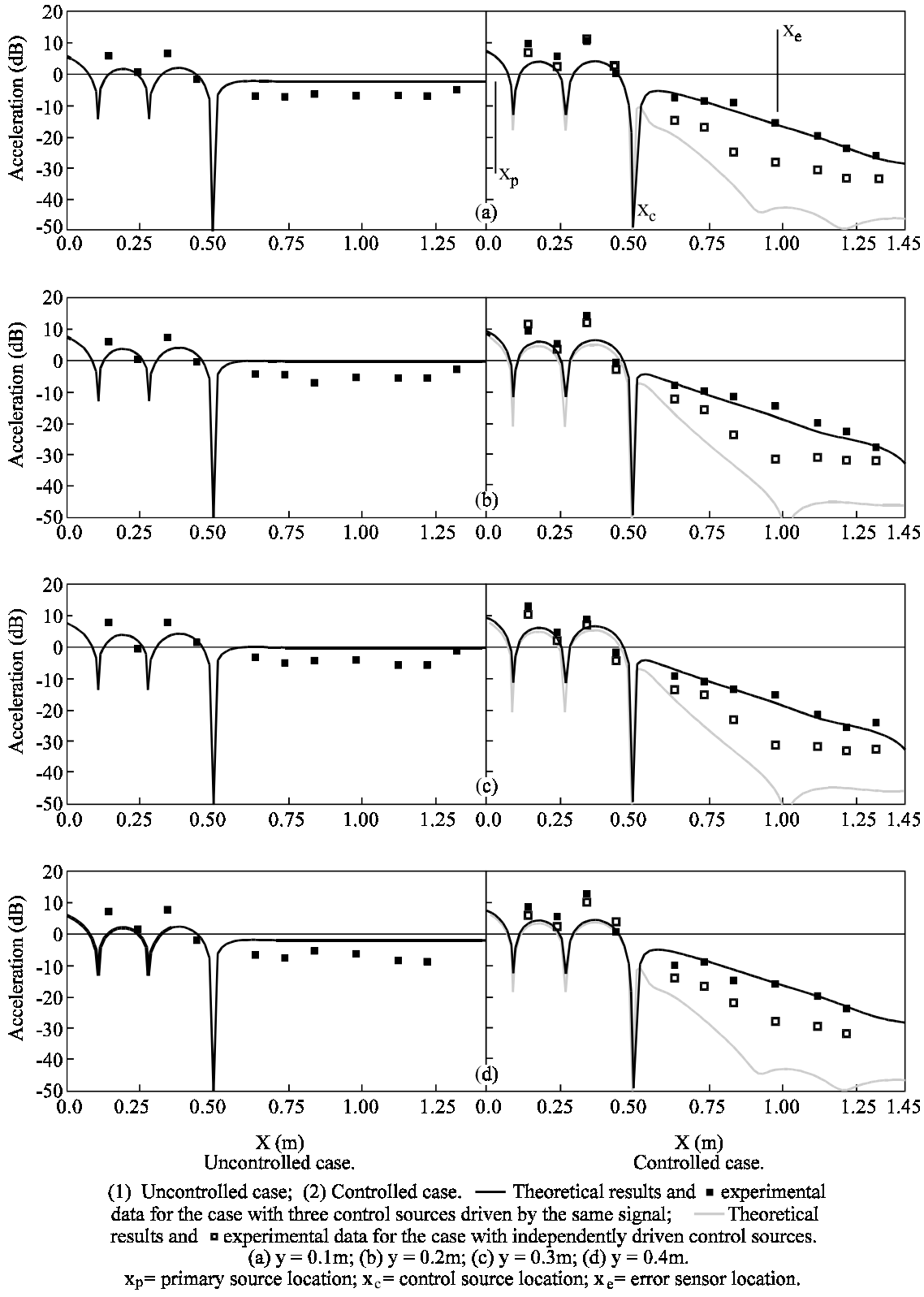

Figure 3.36 Acceleration distributions for the semi-infinite plate.

3.6 SUMMARY

A theoretical model has been developed to describe the vibration response of a stiffened plate to a range of excitation types, and in particular to describe the vibration response of stiffened plates to point force primary excitation sources and angle stiffener and piezoceramic stack control sources. The numerical results indicate that flexural vibrations in plates can be actively controlled using piezoceramic stack actuators placed between the flange of an angle stiffener and the plate surface. Numerical results also indicate:

(1) The mean amplitude of the control forces required for optimal control generally decreases with increasing frequency.

(2) The optimum control forces are either in phase or 180^{o} out of phase with the primary sources. This is true for the semi-infinite plate as well as the finite plate, because a standing wave is generated by the vibration reflections from the finite end and the angle stiffener.

(3) Maxima occur in the mean control source amplitude required for optimal control when the separation between control and primary forces is given by $x = (c + nx_s)$ where n is an integer, c is a constant dependent on frequency, and x_s is the axial separation between standinng wave nodes. These maxima occur when the control sources are located at a nodal line in the standing wave generated by reflection from the plate termination and the angle stiffener. Minima in the mean attenuation of acceleration level downstream of the

error sensor occur when the control sources are located at a nodal line in the standing wave.

(4) Increasing the separation between the primary and control sources does not improve attenuation.

(5) The amount of attenuation achieved downstream of the error sensors increases with increasing separation between the error sensors and the control sources.

(6) When the line of error sensors is located at a nodal line in the standing wave that exists in finite plates, the attenuation achieved is less than that achieved with the error sensors located away from a node. Locating the error sensors at a node does not affect the amplitude of the control sources required for optimal control.

(7) A second set of control sources can be used to overcome the difficulty in controlling vibration when the first set of control sources is located at a nodal line in a standing wave. The maxima in mean control source amplitude and the minima in attenuation that occur when the first set of control sources are located at a standing wave nodal line are eliminated in this way.

(8) At low frequencies, there is very little difference in the mean control effort required for optimal control and the mean attenuation downstream of the line of error sensors

achieved between control using independent control sources and control sources driven by a common signal. When higher order across-plate modes become significant, very little attenuation is achieved with control sources driven by a common signal. Good reduction in acceleration level is achieved with independently driven control sources right across the frequency range considered.

(9) Numerical results indicated that three control actuators and three error sensors were sufficient for optimally controlling vibration in the plate considered at the frequency considered.

The theoretical model outlined was verified experimentally for the plate with simply supported sides, one end free and the other end anechoically terminated. A modal analysis of the plate indicated that the anechoic termination allowed some reflection and so did not exactly model the ideal infinite end, and that the angle stiffener made a significant difference to the vibration response of the plate. Comparison between experimental results and theoretical predictions for the vibration of the plate with and without active vibration control showed that:

(1) The theoretical model accurately predicted the vibration response of the plate for the uncontrolled case and the case with control sources driven by the same signal. The angle stiffener reflected more of the vibration and transmitted less than the theoretical model predicted.

(2) The theoretical model predicted more attenuation that could be achieved experimentally for the case with independently driven control sources. An error analysis indicated that an error in the control source signal of 0.1% would produce a decrease in attenuation corresponding to the difference between the theoretical prediction and the experimental result. Nevertheless, around 25 dB attenuation was achieved experimentally for the case with independently driven control sources.